JNeurosci Accepted Manuscript

JNeurosci
THE JOURNAL OF NEUROSCIENCE

Research Articles: Cellular/Molecular

Microglial mTOR is neuronal protective and anti-epileptogenic in the pilocarpine model of temporal lobe epilepsy

https://doi.org/10.1523/JNEUROSCI.2754-19.2020

Cite as: J. Neurosci 2020; 10.1523/JNEUROSCI.2754-19.2020

Received: 19 November 2019
Revised: 5 August 2020
Accepted: 24 August 2020

This Early Release article has been peer-reviewed and accepted, but has not been through the composition and copyediting processes. The final version may differ slightly in style or formatting and will contain links to any extended data.

Alerts: Sign up at www.jneurosci.org/alerts to receive customized email alerts when the fully formatted version of this article is published.

Copyright © 2020 the authors

JNeurosci Accepted Manuscript

Title: Microglial mTOR is neuronal protective and anti-epileptogenic in the pilocarpine model of temporal lobe epilepsy.

Abbreviated title: Microglial mTOR in neuronal loss and epilepsy

Xiao-Feng Zhao[1,5,*], Yuan Liao[2,*], Mahabub Maraj Alam[1], Ramkumar Mathur[2], Paul Feustel[1], Joseph E. Mazurkiewicz[1], Matthew A. Adamo[3], Xinjun Cindy Zhu[2,4], Yunfei Huang[1,5]

1. Department of Neuroscience and Experimental Therapeutics, Albany Medical College, Albany, New York 12208
2. Department of Molecular and Cellular Physiology, Albany Medical College, Albany, New York 12208
3. Department of Neurosurgery, Albany Medical College, Albany, New York 12208
4. Department of Medicine, Albany Medical College, Albany, New York, 12208
5. Lead contact/correspondence: Zhaox1@amc.edu; huangy@amc.edu

* Authors share co-first authorship.

Number of pages: 36

Number of figures: 9

Number of tables: 2

Number of multimedia: 0

Number of words for abstract: 149

Number of words for introduction: 701

Number of words for discussion: 1843

Conflict of interest statement: The authors declare no competing financial interests.

Acknowledgements: This work was supported by NIH grant NS093045 and NS112713 to YH.

JNeurosci Accepted Manuscript

Abstract

Excessive activation of mTOR signaling is epileptogenic in genetic epilepsy. However, the exact role of microglial mTOR in acquired epilepsy remains to be clarified. In the present study, we found that mTOR is strongly activated in microglia following excitatory injury elicited by status epilepticus. To determine the role of microglial mTOR signaling in excitatory injury and epileptogenesis, we generated mice with restrictive deletion of mTOR in microglia. Both male and female mice were used in the present study. We found that mTOR-deficient microglia lost their typical proliferative and inflammatory responses to excitatory injury, whereas the proliferation of astrocytes was preserved. In addition, mTOR-deficient microglia did not effectively engulf injured/dying neurons. More importantly, microglial mTOR-deficient mice displayed increased neuronal loss and developed more severe spontaneous seizures. These findings suggest that microglial mTOR plays a protective role in mitigating neuronal loss and attenuating epileptogenesis in the excitatory injury model of epilepsy.

JNeurosci Accepted Manuscript

Significance statement

The mTOR pathway is strongly implicated in epilepsy. However, the effect of mTOR inhibitors in preclinical models of acquired epilepsy is inconsistent. The broad presence of mTOR signaling in various brain cells could prevent mTOR inhibitors from achieving a net therapeutic effect. This conundrum has spurred further investigation of the cell-type-specific effects of mTOR signaling in the CNS. We found that activation of microglial mTOR is anti-epileptogenic. Thus, microglial mTOR activation represents a novel anti-epileptogenic route that appears to parallel the pro-epileptogenic route of neuronal mTOR activation. This may explain why the net effect of mTOR inhibitors is paradoxical in the acquired models of epilepsy. Our findings could better guide the use of mTOR inhibitors in preventing acquired epilepsy.

Keywords

Microglia; mTOR; epilepsy; phagocytosis; excitatory neuronal injury; spontaneous recurrent seizures

JNeurosci Accepted Manuscript

Introduction

Epileptogenesis is a pathological process that transforms a normal brain into an epileptic brain, typically initiated by genetic mutations and neurological insults such as status epilepticus (SE). Excessive activation of mTOR signaling is recognized as a pathomechanism underlying both genetic and acquired epilepsy (Crino, 2016; D'Gama et al., 2015; Talos et al., 2018; Wong, 2013). Modeling of mTOR hyperactivation in rodents demonstrates a very robust epileptogenic effect (Carson et al., 2012; Feliciano et al., 2011; McMahon et al., 2012; Meikle et al., 2007; Nguyen et al., 2019; Orlova et al., 2010; Sunnen et al., 2011; Uhlmann et al., 2002; Zeng et al., 2009; Zhang et al., 2016). However, over the past decade, mTOR inhibitors have been found to have very minimal or inconsistent effects in preventing acquired epilepsy (Buckmaster et al., 2009; Gericke et al., 2019; Zeng et al., 2009). As mTOR is expressed ubiquitously in neuronal and non-neuronal cells and its mode of action is very wide-ranging, it is perhaps not surprising that the outcomes from broad mTOR inhibition are less than desirable. Therefore, it is of paramount importance to further dissect the cell-specific roles of mTOR signaling in epileptogenesis so as to develop better anti-epilepsy strategies. Previous studies mainly focused on modeling hyperactivation of mTOR signaling in neurons and astrocytes, which nicely recapitulates the epileptogenic activity (Meikle et al., 2007; Uhlmann et al., 2002). The role of microglia and microglial mTOR signaling in epileptogenesis has only recently been increasingly explored (Abraham et al., 2012; Boer et al., 2008; Mo et al., 2019; Schartz et al., 2018; Sierra et al., 2010; Zhao et al., 2018).

Microglia are generally considered to be resident macrophages. They are the main innate immune cells in the CNS and the principal producer of pro-inflammatory cytokines in response to brain injury (Wolf et al., 2017). In addition to their innate immune activity, microglia also play various roles in brain development and CNS homeostasis through processes such as synapse pruning, clearing of apoptotic cells, and repair of minute insults (Nimmerjahn et al., 2005; Paolicelli et al., 2011; Sierra et al., 2013). Microglia also regulate myelination (Miron, 2017; Wlodarczyk et al., 2017) as well as proliferation and activation of astrocytes (Liddelow et al., 2017). Microglia become activated in response to epileptic insults (Boer et al., 2006; Eyo et al., 2016; Schartz et al., 2018; Zhang et al., 2016) and their inflammatory response has long been postulated to be epileptogenic (Aronica et al., 2017; Quan et al., 2013; Vezzani and Viviani, 2015). Morphologically reactive microglia have been found in the brains of animal models of temporal lobe epilepsy (TLE) (Brewster et al., 2013; van Vliet et al., 2012) and in surgical

JNeurosci Accepted Manuscript

resections of epilepsy patients (Beach et al., 1995; Liu et al., 2014; Sosunov et al., 2012). Pharmacological inhibition of microglial activation appears to attenuate epileptogenesis (Abraham et al., 2012). The pro-inflammatory action of microglia is postulated to be an etiologic driver of epileptogenesis. We recently discovered an alternative epileptogenic process involving microglia which is independent of an inflammatory response (Zhao et al., 2018).

mTOR signaling was found to be elevated in microglia in human epileptic resections (Nonoda et al., 2009; Sosunov et al., 2012) and a preclinical model (Brewster et al., 2013). Pharmacological inhibition of mTOR by rapamycin suppresses microglial activation and/or proliferation (Brewster et al., 2013; Nguyen et al., 2015; van Vliet et al., 2016), while other studies reported that the mTOR pathway may have inconsistent effects on microglia activation (van Vliet et al., 2012) or the effect on epileptogenesis was driven by unintended activation of mTOR signaling in neurons and astrocytes (Zhang et al., 2018). mTOR signaling was reported to regulate microglial behavior via several other mechanisms (Kassai et al., 2014; Li et al., 2016; Shen et al., 2016; Shibuya et al., 2014). Our recent study revealed that mice with excessive activation of mTOR restrictively in microglia develop spontaneous recurrent seizures, suggesting a pro-epileptogenic role of up-regulated microglial mTOR (Zhao et al., 2018; Zhao et al., 2019). However, the exact role of activated microglial mTOR in epileptogenesis in acquired epilepsy remains to be determined. In the present study, we generated Cx3cr1-cre;mTOR$^{f/f}$ mice to probe the role of microglial mTOR signaling in epileptogenesis in response to status epilepticus (SE).

Experimental Procedures

Animals

Tg(Cx3cr1-cre)MW126Gsat/Mmucd (Cx3cr1-cre) mice were acquired from the MMRRC (Zhao et al., 2018; Zhao et al., 2019), *B6.129S4-Mtor$^{tm1.2Koz}$/J* (mTOR$^{f/f}$) mice were acquired from The Jackson Laboratory. Both sexes were used. Animals were housed in a pathogen-free, temperature- and humidity-controlled facility with a 12-h light cycle (lights on at 7:00 A.M.) and given *ad libitum* access to food and water. All experiments were performed according to the guidelines set by the Institutional Animal Care and Use Committee as well as the National Institutes of Health *Guide for the Care and Use of Laboratory Animals*. Efforts were made to minimize suffering and unnecessary use of animals.

JNeurosci Accepted Manuscript

Pilocarpine treatment

Status epilepticus (SE) was induced by pilocarpine as described in our previous work (Zhao et al., 2019). In brief, to minimize the peripheral cholinergic side effects of pilocarpine, 8- to 10-week-old mice of either sex were first injected intraperitoneally with 1 mg/kg methyl scopolamine (*Sigma-Aldrich*) in 0.9% NaCl for 10 min before injection of pilocarpine (*Sigma-Aldrich*). For all groups, pilocarpine administration was started at the same time of day, 9 A.M. to 3 P.M. $mTOR^{Cx3cr1\text{-}creCKO}$ mice and their controls ($mTOR^{f/f}$) from the same litter were used for the experiments. There is a variation in seizure threshold to the convulsant pilocarpine between control and knockout mice or even within control mice from the same litter. To induce comparable levels of SE among mice, we used a modified ramping-up pilocarpine injection protocol. We treated mice with an initial dose of pilocarpine at 200mg/kg by intraperitoneal injection, followed by 50mg/kg every 15 min until the onset of stage-4 or -5 seizures. Seizures were classified according to the Racine scale (Racine, 1972), with modifications made by Borges et al. (Borges et al., 2003): stage 0, normal activity; stage 1, rigid posture or immobility; stage 2, stiffened, extended and often arched tail; stage 3, partial body clonus, including forelimb or hindlimb clonus or head bobbing; stage 4, whole body continuous clonic seizures with rearing; stage 5, severe whole-body continuous clonic seizures with rearing and falling; stage 6, tonic-clonic seizures with loss of posture or jumping. Animals were allowed to develop SE for 4 h. The total time of seizures at Racine scale 3 and above was recorded. The mortality rates to pilocarpine treatment were 60.7 ± 11.4% and 53.3 ± 11.3% for control and $mTOR^{Cx3cr1\text{-}creCKO}$ mice, respectively. The surviving pilocarpine-treated animals were assigned to each group by pairing animals based on total seizure duration to ensure that the overall severity of SE induced by pilocarpine in each group was comparable. To further ensure that the animals started with a similar intensity of SE to pilocarpine treatment, animals that developed mild seizures (defined as total seizure duration less than 50% of average) were excluded from further study. SE was terminated by diazepam treatment (*Sigma*) (10 mg/kg, i.p.), followed by administration of a single dose of dextrose (1.5 g/kg, i.p.). Animals were placed on a 30°C warm pad for recovery for 1 h.

Rapamycin treatment

Rapamycin treatment was performed as previously described (Huang et al., 2010). In brief, wild-type mice (mixed background, *C57BL/6NJ*) were first treated with pilocarpine to allow SE for 4 h, immediately followed by intraperitoneal injection of either vehicle (5% Tween-20 and 4% ethanol) or rapamycin (LC Laboratories; 6 mg/kg/day). Mice then received two additional doses

JNeurosci Accepted Manuscript

of rapamycin 24 h apart. Mouse brain samples were harvested and processed for further analysis.

Immunohistochemistry and acquisition of images

Animals were anesthetized with pentobarbital (*Sigma*) (100 mg/kg, i.p) and transcardially perfused with PBS followed by 4% paraformaldehyde (PFA) in PBS, pH 7.4. Brains were post-fixed overnight in 4% PFA buffer, followed by cryoprotection in 30% sucrose in PBS for at least 48 h. Mouse brains were then embedded in Neg-50^{TM} frozen section medium (*Fisher Scientific*), and sectioned on a cryostat at 35 µm-thickness for all histological analyses unless otherwise described. For most immunohistological experiments, unless otherwise specified, brain sections were washed with PBS, blocked and permeabilized in 10% BSA (*Sigma*) and 0.3% Triton X-100 (*Sigma*) in PBS at room temperature for 2 h. Sections were incubated with primary antibodies in the blocking buffer overnight at 4 °C, and then washed with PBS for 5 min and repeated 3 times, followed by incubation with appropriate fluorescent conjugated secondary antibodies for 2 h at room temperature. For staining of activated caspase-3, brain sections were permeabilized with 0.5% Tween 20. For staining with goat anti-Iba1 (1:250; catalog #NB100-1028; Novus Biologicals), free-floating sections were permeabilized and blocked with blocking buffer containing 0.3% Triton X-100 and 5% normal donkey serum in PBS at room temperature for 1 h. Sections were then incubated with goat anti-Iba1 antibody diluted in blocking buffer overnight at 4°C. Nuclei were counterstained with DAPI (*Sigma*) and coverslips were applied with Fluoromount G (*Southern Biotech*), and sealed with nail polish. Images were acquired using a Zeiss LSM 880 confocal microscope with Airyscan and processed with Zen black 2.1 or Zen blue lite 2.3 (*Carl Zeiss*). Immunofluorescence signals were quantified using the NIH image analysis software ImageJ.

Brain coronal sections with similar anatomical locations (near bregma -2 mm position based on the mouse brain atlas) from all groups of control and *mTOR*$^{Cx3cr1\text{-}cre}$CKO mice were selected for all histological analyses. To show the staining of microglia, astrocytes and neurons in the entire cortex and hippocampus, images were acquired using the tiles and positions module and a 25× water objective lens. For the quantification of microglia density, brain sections were stained with anti-Iba1 (*Wako*), anti-CD68 (*Bio-Rad*), and DAPI (*Sigma*). For evaluating the proliferation of microglia, microglia were co-labeled with anti-Iba1 (Wako) and anti-Ki67 (*Abcam*). For the quantification of astrocyte density, brain sections were stained with anti-Iba1 (*Wako*), anti-GFAP (*Millipore-Sigma*), and DAPI. For the quantification of cleaved-Caspase3-positive cell density,

JNeurosci Accepted Manuscript

brain sections were stained with anti-cleaved-Caspase3 (*Cell Signaling*) and DAPI (*Sigma*). Confocal image stacks were collected using a 25× water objective lens with a 1-μm interval through a 10-μm z-depth of the tissue under the tiles and stitching mode covering an area of 1656 μm × 3250 μm. The image stacks were subjected to maximum intensity projection to create 2D images and then imported into Neurolucida software (*MBF Bioscience*, Williston, VT) for cell number counting. Microglia within the areas of the M1 motor cortex around layer IV, the hippocampal radiatum layer adjacent to pyramidal CA1, the stratum lucidum adjacent to CA3, and dentate gyrus (hereafter referred to as cortex, CA1, CA3, and DG) were quantified. Data are presented as the number of Iba1-positive cells per mm^2. For the quantification of immunostaining intensity of CD68, all images were acquired and processed with identical parameter settings. Immunofluorescence intensity was quantified using the NIH image analysis software ImageJ.

Fluoro-Jade B staining

FJB staining was used to evaluate the acute excitatory injury triggered by SE. The sections were mounted on 2% gelatin-coated slides and then air dried on a slide warmer at 50 ˚C for at least 30 min. The slides were first immersed in a solution containing 1% sodium hydroxide in 80% alcohol (20 mL of 5% NaOH added to 80 mL absolute alcohol) for 5 min. This was followed by 2 min in 70% alcohol and 2 min in distilled water. The slides were then transferred to a solution of 0.06% potassium permanganate on a shaker table for 10 min. The slides were then rinsed in distilled water for 2 min. After 20 min in 0.0004% Fluoro-Jade® B staining solution (*Histo-Chem Inc*.), and 50 μg/ml DAPI (*Sigma*) in 0.1% acetic acid, the slides were rinsed in three changes of distilled water, 1 min each. Excess water was removed by briefly (about 15 s) draining the slides vertically on a paper towel. The slides were then placed on a slide warmer, set to approximately 50 ˚C, until they were fully dry (5-10 min). The dry slides were cleared by immersion in xylene for at least 1 min before cover slipping with DPX (Sigma-Millipore, #06522). FJB-stained slices were imaged using a Zeiss AxioImager M2 microscope system paired with Neurolucida & Stereo Investigator software packages. In brief, the Cy2 channel (for the green signal of FJB) and the DAPI channel (for DAPI) were selected. A region of interest (ROI; the whole hippocampus area) was traced by using a 5× objective lens (5×/NA 0.16). The ROI was then scanned in a multi-sites pre-focused model by using a 20× objective lens (20×/NA 0.80). The final images were saved in TIFF format for later analysis. The FJB-positive cells were counted using Neurolucida with an identical pre-set threshold among the compared groups.

JNeurosci Accepted Manuscript

Analysis of *in vivo* phagocytosis

In vivo phagocytosis analysis was performed as previously described (Abiega et al., 2016; Zhao et al., 2018). In brief, brain sections were stained with anti-Iba1 (*Wako*) and DAPI (*Sigma*), and confocal image stacks were collected using a 40× oil objective lens with a 0.2-μm interval through a 20-μm z-depth of the tissue under the tiles and stitching mode covering cortex and CA1 areas of 211.7 μm × 636.8 μm. Dying cells were recognized as cells showing a condensed and/or fragmented nuclear morphology after DAPI staining. To quantify microglial phagocytosis of dying cells, the enclosed pouches formed by microglial processes wrapping around dying cells were counted. Then, phagocytosis capacity was calculated by applying the following formula: Phagocytosis capacity = [(1Ph1+2Ph2+3Ph3 … +nPhn)/MG]% (where Phn is the number of microglial cells with n phagocytic pouches; MG is the total number of microglia cells). For each mouse, three coronal 35-μm sections that were approximately 105 μm apart (i.e., every 4th section) and from similar anatomical locations (near bregma -2 mm position based on the mouse brain atlas) were selected for histological analysis.

Analysis of synapse density

Synapses were quantified according to the protocol previously described (Zhao et al., 2018). Brain tissues were sectioned at 15-μm thickness. Three sections at equidistant planes (100 μm apart) per mouse were used for subsequent co-immunostaining with antibodies against the pre-synapse protein VGlut2 (*EMD Millipore*) and the post-synapse protein Homer1 (*EMD Millipore*) for excitatory synapses, and the pre-synapse protein VCAT (*Synaptic Systems*) and the post-synapse protein Gephyrin (*Synaptic Systems*) for inhibitory synapses. In brief, for staining of excitatory synapses, brain sections were incubated in blocking buffer (0.3% Triton X-100 and 10% BSA in 1X PBS) for 1 h at room temperature and then incubated in primary antibody solution (0.3% Triton X-100 and 10% BSA in 1X PBS; anti-VGlut2 1:4000, anti-Homer1 1:4000) at 4°C for 48 h. For staining of inhibitory synapses, brain sections were incubated in blocking buffer (0.2% Triton X-100 and 5% normal goat serum in 1X PBS) for 1 h at room temperature and then incubated in primary antibody solution (0.2% Triton X-100 and 3% normal goat serum in 1X PBS; anti-VGAT 1:4000, anti-Gephyrin 1:4000) at 4°C for 48 h. Brain sections were washed for 20 min for 3 times, followed by incubation with fluorophore-conjugated secondary antibodies at room temperature for 1 h. Nuclei were counterstained with DAPI (Sigma) and coverslips were applied with Fluoromount G (Southern Biotech), and sealed with nail polish. The stained sections were imaged within 48 h of staining with a 63× Zeiss pan-Apochromat oil, 1.4 NA objective lens on a Zeiss LSM 880 with the Airyscan protocol in super-resolution mode. Two

JNeurosci Accepted Manuscript

images with maximum synaptic staining within a z-stack of 21 serial optical frames (0.3 μm interval) were selected for quantification. Six single images per mouse brain were analyzed. Synapses were identified as yellow punctae, which represent the co-localization of VGlut2 (green) and Homer1 (red) or VCAT (green) and Gephyrin (red). The number of synapses in the areas including the M1 motor cortex around layer IV and the hippocampal radiatum layer adjacent to pyramidal CA1 were counted using Image J software (version 1.51f, *NIH*).

Three-dimensional reconstruction of microglia

For microglial cell three-dimensional reconstruction, 35-μm coronal brain sections were stained with anti-Iba1 (*Wako*) as described (Zhao et al., 2018). Confocal image stacks were collected using a 63× oil objective lens with a 0.2-μm interval through a 20-μm z-depth of the tissue under the tiles and stitching mode covering cortex (CTX), hippocampus CA1 and CA3, and dentate gyrus (DG) areas of 256.41 μm × 256.41 μm. For each mouse, three coronal 35-μm sections that were approximately 105 μm apart (i.e., every 4th section) and from similar anatomical locations (near bregma -2 mm position based on the mouse brain atlas) were selected for imaging and further analysis using IMARIS software (Bitplane). For three-dimensional reconstruction using IMARIS software (Bitplane), microglia cells were traced/reconstructed by following the vendor's instructions. In brief, for microglial cell volume evaluation, the Surfaces module of IMARIS was used to reconstruct cells and to automatically analyze cell volume. For evaluating microglia dendrite length, number of branch points, number of terminal points and number of segments, the Filaments module of IMARIS was used to trace and reconstruct cells, and to further perform automatic analyses. All settings used for the reconstruction were identical between the control and the *mTOR*$^{Cx3cr1\text{-}cre}$*CKO* groups.

TUNEL staining

TUNEL staining was performed using the TMR-red kit (*Roche*) following the manufacturer's instructions. In short, tissue sections were fixed with fixation solution (4% paraformaldehyde in PBS, pH 7.4, freshly prepared) for 20 min and then washed with PBS for 30 min at room temperature. The slides were incubated in permeabilization solution (0.1% Triton X100, 0.1% sodium citrate, freshly prepared) for 2 min on ice (2 to 8°C). After two rinses with PBS, the brain sections were incubated with 50 μl of TUNEL reaction mixture and placed in a humidified chamber for 60 min at 37°C in the dark. The slides were washed with PBS three times for 5 min each, then counterstained with DAPI. TUNEL staining was imaged using a Zeiss LSM 880 confocal microscope with Airyscan and processed with Zen black 2.1 or Zen blue lite 2.3 (*Carl*

JNeurosci Accepted Manuscript

Zeiss). For evaluating the ratio of TUNEL/cleaved-Caspase3-positive cells to FJB-positive cells, three adjacent sections of each group were picked and stained separately with FJB, TUNEL and cleaved-caspase3. Images were acquired and cell numbers were counted by using Neurolucida. The ratio was calculated by dividing the TUNEL/cleaved-Caspase3 positive cell number with the FJB-positive cell number.

Nissl (Cresyl Violet) staining

Brain sections were mounted onto gelatin-subbed slides (*SouthernBiotech*) and dried at room temperature for 2 h. Prior to staining, the Cresyl violet staining solution was made by combining 30 ml of the Cresyl violet stock solution (0.2 g Cresyl violet-acetate in 150 ml distilled water) (*Sigma*) with 300 ml buffer solution, pH 3.5 (282 ml of 0.1 M acetic acid combined with 18 ml of 0.1 M sodium acetate). The Cresyl violet staining solution was pre-warmed in an incubator for at least 1 h at 60 ˚C prior to staining. Then, the brain sections were stained as follows: 1) xylene, 5 min; 2) 95% alcohol, 3 min; 3) 70% alcohol, 3 min; 4) deionized distilled water, 3 min; 5) Cresyl violet staining solution at 60 ˚C, 10 min; 6) distilled water, 3 min; 7) 70% alcohol, 3 min; 8) 95% alcohol, 1 min; 9) 100% alcohol, 3 dips; 10) xylene, 5 min; 11) xylene, 30 min. After finishing all the steps, the slides were covered with DPX (*Sigma*) and sealed with nail polish. For imaging of Nissl-stained slides, the color mode of the Zeiss AxioImager M2 microscope system paired with Neurolucida was selected. A region of interest (ROI; the whole hippocampus area) was traced using a 5× objective lens (5×/NA 0.16). After switching the objective lens to 20× (20×/NA 0.80), white balance and background subtraction were performed and the ROI was then scanned using a multi-sites pre-focused model. The final images were saved in TIFF format for later analysis.

***In vitro* phagocytosis assay**

Cultured microglia were seeded onto poly-D-lysine-coated 35-mm culture dishes with glass-bottoms at 0.5×10^5 cells/dish (*MatTek*) 1-2 days prior to the assay. pHrodo® Green zymosan bioparticles (*ThermoFisher*) were dissolved at 0.5 mg/mL in phenol red-free DMEM (*Life Technologies*), vortexed and sonicated to homogeneously disperse the particles immediately before the assay. Prior to live imaging, the culture medium was removed and the culture dish was washed once with pre-warmed phenol red-free DMEM, and then 100 µl of bioparticle suspension was added to the area with the glass-bottom. The microscope stage incubator was pre-set to 37 °C and the environmental chamber filled with 5% CO2. Immediately following the

JNeurosci Accepted Manuscript

addition of the bioparticles, a series of image frames was acquired at 1 frame/min for 61 frames (Zhao et al., 2018).

Purification of microglia from mouse brains

Mice were anesthetized with pentobarbital (100 mg/kg, i.p) and quick-perfused with 30 ml PBS without Ca2+ and Mg2+. Mouse brains were dissected into 5-ml round-bottom tubes (1 brain/tube) (*Falcon*) pre-filled with 1 ml serum-free medium (DMEM/F12 with 4.5 mg/ml glucose) and 1 ml dissociation medium (DMEM/F12 plus 1 mg/ml papain and 1.2 U/ml dispase II, and DNase I to 20 U/ml) prepared immediately before use, and homogenized using a 3-ml syringe plunger (*BD Bioscience*). After adding an additional 2 ml of dissociation medium, the suspension was transferred into a new 15-ml tube and incubated at 37 °C for 10 min. Then, 3 ml of neutralization medium (DMEM/F12 with 4.5 mg/ml glucose and 10% FBS) was added to each tube to stop the digestion. The suspension was further dissociated by pipetting up and down for 10-15 rounds with a 1-ml pipet tip touching the bottom of the 15-ml tube, and then passed through a 30-μm cell strainer (*Miltenyi*). Myelin was removed by adding an equal volume of 70% Percoll followed by centrifugation at 800 × g at 4 °C for 15 min. Cells were washed once with FACS buffer (1% BSA, 0.1% sodium azide, 2 mM EDTA in PBS, pH 7.4) and then processed for further purification of microglia. We utilized anti-Cx3cr1-PE antibody (*Biolegend*) to bind microglia, followed by addition of anti-PE MicroBeads (*Miltenyi*) to capture bound cells. The entire procedure was based on the manufacturer's instructions. Briefly, dissociated cells (~10^7) were resuspended in 50 μl FACS buffer followed by addition of 1 μl anti-mouse CD16/CD32 (*Biolegend*) and incubation on ice for 10 min to block Fc receptors. The cells were then incubated with primary PE-conjugated antibody according to the manufacturer's recommendations. After washing the cells twice with FACS buffer, the cells were resuspended in 80 μl FACS buffer and 20 μl anti-PE MicroBeads, and incubated at 4 °C for 15 min. The cells were further diluted in 500 μl FACS buffer and passed through a magnetic MS column (*Miltenyi*). After three washes of the column with FACS buffer, the MS column was moved away from the magnetic field to elute the cells from the column with 1 ml FACS buffer.

RNA isolation, RT-PCR, and Real-time PCR

Total RNA was extracted from purified microglia and cultured microglia using TRIzol Reagent (*Life Technologies*) according to the manufacturer's instructions. To isolate RNA from brain tissues, mouse brains were first perfused with 50 ml of PBS prior to dissection of the cortex and hippocampus. Dissected cortical and hippocampal tissues were briefly homogenized in TRIzol

JNeurosci Accepted Manuscript

Reagent, followed by RNA extraction. To better recover total RNA from purified microglia, 0.5 µl RNase-free glycogen at 20 µg/ml (*Roche*) was added to 0.5 ml TRIzol extraction volume prior to RNA precipitation with isopropanol. RNA pellets were resuspended in 50 µl of RNase-free water (*Fisher Scientific*) and incubated at 55°C for 10 min. RNA concentrations were determined by using a SmartSpec Plus Spectrophotometer (*Bio-Rad*). cDNA was synthesized from 0.2-1 µg of total RNA via reverse transcription using a Verso cDNA Synthesis Kit (*Thermo Scientific*) in a total volume of 20 µl. The cDNA templates were further diluted 2-3 times in water. Two microliters of diluted templates were used for real-time PCR. RT-PCR was performed in a 96-well PCR plate (*Bio-Rad*) using a SYBR Green qPCR Master Mix kit (*Applied Biosystems*) in a Step One Plus Real-time PCR System (*Applied Biosystems*). Each sample was evaluated in triplicate. The CT value was used to calculate the fold change of RNA abundance after normalization to GAPDH. All primer sequences are provided in Table 2.

Video/EEG recording of spontaneous seizures

Video/EEG recording was done according to previously published work (McMahon et al., 2012; Zhao et al., 2018). One week after SE, mice were implanted epidurally with three-channel EEG electrodes (*Plastics One*). After another week of recovery from the electrode implantation surgery, the electrodes were connected to the video/EEG system (*DataWave Technologies*) and monitored 24 h per day for up to 60 days. All video/EEG data were analyzed by trained researchers blinded to the genotypes. EEG seizure events were characterized by the sudden onset of high-frequency and high-amplitude (>2-fold background) activity and a duration greater than 10 seconds, along with characteristic postictal suppression. All electrographic seizures were verified behaviorally by video data to exclude movement artifacts.

Statistical analysis

Data were analyzed using Graphpad Prism 7 software with appropriate tests for comparisons between the control and *mTOR*$^{Cx3cr1\text{-}cre}$*CKO* mice. G-Power was used for power analysis. Sample sizes were calculated to determine the minimum number of animals for adequate study power in order to detect the differences among groups. For immunohistological analysis, we observed that the readouts for the differences of the number of p-S6-positive microglia, the density of microglia, and phagocytosis activity between the compared groups (i.e. sham-treated versus SE and control versus *mTOR*$^{Cx3cr1\text{-}cre}$*CKO)* are consistent and robust. Our preliminary calculation found the co-efficient of determination to be 0.9-0.95. We set α at 0.05, and power at 95%. A sample size of 4-5 is adequate. One-way ANOVA, followed by Tukey's multiple

JNeurosci Accepted Manuscript

comparisons test was used to test the significance of differences among three experimental groups. Student's t test was used to test the significance of differences between the control group and the *mTORCx3cr1-creCKO* group. Two-way ANOVA, followed by Sidak test, was used for the comparison of the time course for *in vitro* phagocytosis between the control and mTORCx3cr1-creCKO groups. For analysis of spontaneous seizures, we set the co-efficient of determination at 0.6, yielding a sample size of 21. The chi-square test was used to test the percentage difference of SRS between the control and *mTORCx3cr1-creCKO* groups. The Mann-Whitney test was used for testing the difference in seizure duration and number of cumulative seizure events between control and $mTOR^{Cx3cr1}$CKO mice. A p value of < 0.05 was considered significant.

All key resources related to the experimental procedures are listed in Table 1 and 2

Results

Increased levels of pS6 in activated microglia

Previous studies revealed that the levels of p-S6, an *in vivo* mTOR activation marker, are elevated following SE induced by either pilocarpine or kainic acid in animal models of TLE (Brewster et al., 2013; Huang et al., 2010; Zeng et al., 2009). In the present study, we performed IHC to characterize the expression of p-S6 in the cortex and hippocampus. Microglia of sham-treated animals expressed very low levels of p-S6 (Fig. 1A-1B). However, we observed robust p-S6 expression in morphologically activated microglia in both the cortex and hippocampus 3 days post-SE (Fig. 1A-1B). Nearly 50% of $Iba1^+$ cells were p-S6 positive. Treatment with the mTOR inhibitor rapamycin markedly reduced p-S6 expression (Fig. 1A-1B), consistent with the finding that mTOR signaling is activated in microglia in response to neuronal injury induced by SE (Brewster et al., 2013). CD68 is an indicator of microglia activation. Rapamycin also reduced the induction of CD68 (Fig. 1A & 1C).

mTOR deletion impairs activation and proliferation of microglia

To examine the role of mTOR in microglia, we generated $mTOR^{Cx3cr1\text{-}cre}$CKO mice to delete mTOR in microglia by crossing $mTOR^{f/f}$ and Cx3cr1-cre lines. Our recent studies have verified that the Cx3cr1-cre line is microglial specific (Zhao et al., 2018; Zhao et al., 2019). In our previous study, excessive activation of microglial mTOR in TSC1KO mice caused a marked

JNeurosci Accepted Manuscript

change in morphology and increased proliferation of microglia (Zhao et al., 2018). In mTOR$^{Cx3cr1\text{-}cre}$CKO mice, microglia with mTOR deletion became less ramified and displayed moderate morphological changes, including a smaller cell volume, shorter dendrites, and fewer branches and terminal segment points (Fig. 2A-2C), consistent with a role of mTOR in regulating cell growth and size. However, there was no significant change in the density of microglia (Fig 2A, Fig 3A, 3B and 3E).

Having demonstrated that mTOR signaling is activated in microglia following SE, we next evaluated how mTOR-deficient microglia respond to neuronal injury induced by SE. SE was induced by pilocarpine in mTOR$^{Cx3cr1\text{-}cre}$CKO mice and littermate controls. To determine how microglial mTOR signaling acts in response to excitatory injury, we carefully performed dosing of pilocarpine. Our goal was to induce comparable seizures in both groups so that we could determine how control and mTOR$^{Cx3cr1\text{-}cre}$CKO mice respond to excitatory injury. Mice were treated with a single dose of pilocarpine at 200 mg/kg followed by 50 mg/kg every 15 min via intraperitoneal injection until they developed SE. mTOR$^{Cx3cr1\text{-}cre}$CKO mice appeared to require a moderately lower dose of pilocarpine to induce SE compared to their littermate controls (Fig. 3D). Nevertheless, all mice experienced four hours of SE and then were treated with a single dose of diazepam to terminate the seizures. Mouse brains were harvested on days 1, 3, and 7 post-SE. Mouse brain sections were first stained with Fluoro-Jade B (FJB) to evaluate the extent of neuronal injury (Fig. 3A & 3B). Mouse brains that displayed comparable FJB staining in control and mTOR$^{Cx3cr1\text{-}cre}$CKO mice were paired and brain sections adjacent to the sections were used for FJB staining for further analysis of microglia activation. This approach ensures that the animals experienced a similar level of injury because we are examining how microglia respond to neuronal injury. In control mice, we observed that microglia became morphologically less ramified and began to show a significant increase in microglial density on day 3 post-SE, and continued to increase on day 7 post-SE (Fig. 3A, 3B & 3E). In contrast, in mTOR$^{Cx3cr1\text{-}cre}$CKO mice there was only a moderate increase in microglial density on days 3 and 7 post-SE. In control mice, CD68 induction in microglia became prominent within day 1 post-SE, reached a peak on day 3 post-SE, and then declined on day 7 post-SE (Fig. 3A, 3B & 3F). However, in mTOR$^{Cx3cr1\text{-}cre}$CKO mice, the induction of CD68 was very minimal on day 1 post-SE, moderate on day 3 post-SE, and largely resolved by day 7 post-SE. These data suggest that mTOR deletion prevents microglia from becoming activated and proliferative in response to excitatory neuronal injury.

JNeurosci Accepted Manuscript

We next performed Ki67 staining to evaluate proliferation of microglia. In control mice, we observed a significant increase of Ki67 staining on day 1 post-SE, reaching a peak on day 3 post-SE, and declining on day 7 post-SE (Fig. 3C & 3G). However, in mTOR$^{Cx3cr1\text{-}cre}$CKO mice, we found a very moderate increase of Ki67 staining on days 3 and 7 post-SE. These data suggest that mTOR-deficient microglia have lost the proliferative response to excitatory neuronal injury.

mTOR deletion impairs microglial phagocytosis

Microglia are the principal phagocytotic cells that engulf and clear dying neurons (Sierra et al., 2013; Wyatt-Johnson and Brewster, 2020). We next evaluated the effect of mTOR deletion on microglial phagocytosis. In response to neuronal injury, microglia migrate close to dying neurons. Their processes wrap around the neurons to form a phagocytotic cup and engulf neurons. We quantified the number of phagocytotic cups as described previously (Abiega et al., 2016; Sierra et al., 2010; Zhao et al., 2018). We observed an increase of phagocytotic cups on days 1-7 post-SE in control mice (Fig. 4A & 4C). However, phagocytotic cup formation was markedly reduced in mTOR$^{Cx3cr1\text{-}cre}$CKO mice, suggesting that mTOR deficiency impairs phagocytosis (Fig. 4A & 4C). The reduction in microglial phagocytosis activity *in vivo* is not attributable to the reduced microglial density, as the data are presented as the number of cups per microglial cell. We next performed an *in vitro* phagocytosis assay to evaluate phagocytotic activity in cultured microglia, an assay that we described previously (Zhao et al., 2018). We found that mTOR deletion significantly reduced the phagocytosis of Zymosan particles by microglia (Fig. 4B & 4D). Together, our data suggest that mTOR deletion down-regulates microglial phagocytosis.

Microglial mTOR deletion impairs the microglial inflammatory response to excitatory injury

We evaluated cytokines in hippocampal tissues. We observed significant induction of TNFα, IL1β, IL6, and IFNβ on days 1 and 3 post SE in hippocampal tissues from control mice (Fig. 5A). However, the induction of TNFα and IL1β was significantly reduced in mTOR$^{Cx3cr1\text{-}cre}$CKO mice. In contrast, the levels of IL6 and IFNβ were elevated in mTOR$^{Cx3cr1\text{-}cre}$CKO mice when compared to control mice. We next analyzed these cytokines in purified microglia (Fig. 5B). In the sham-treated mice, there was no difference in the levels of TNFα, IL1β, IL6, and IFNβ cytokines in microglia prepared from control and mTOR$^{Cx3cr1\text{-}cre}$CKO mice. We observed that TNFα was induced on days 1 and 3 post-SE, and IL1β was induced mainly on day 7 post-SE. These

JNeurosci Accepted Manuscript

inductions were significantly reduced in mTOR$^{Cx3cr1\text{-}cre}$CKO mice. Interestingly, there was no induction of IL6 and IFNβ in microglia. Our data suggest that the elevated level of IL6 is mainly induced by non-microglial cells.

Microglial mTOR deletion exacerbates the loss of neurons

Again, we first performed FJB staining to evaluate neuronal injuries in the hippocampal CA1 region in both control and mTOR$^{Cx3cr1\text{-}cre}$CKO mice. Mouse brain sections which displayed similar levels of injury were paired for immunohistochemistry studies. Astrocytes typically hyper-proliferate following excitatory injury. Accordingly, we evaluated the density of GFAP^{+} astrocytes. Excessive activation of microglial mTOR in TSC1KO mice caused marked proliferation of astrocytes (Zhao et al., 2018). We observed a marked increase in astrocyte density in the cortex and hippocampus following SE in both the control and mTOR$^{Cx3cr1\text{-}cre}$CKO mice, reaching a peak around day 3 post-SE (Fig. 6A-6C). There was no significant difference between the control and mTOR$^{Cx3cr1\text{-}cre}$CKO groups.

In our previous study, excessive activation of microglial mTOR in TSC1KO mice altered the density of synapses (Zhao et al., 2018). We evaluated the impact of mTOR deletion on neurons. We found no significant difference in synapse density in the cortex and hippocampus between control and mTOR$^{Cx3cr1\text{-}cre}$CKO mice (Fig. 7A & 7B). Pyramidal neurons began to be TUNEL positive at day 1 post-SE, reaching a peak by day 7 in both the control and mTOR$^{Cx3cr1\text{-}cre}$CKO mice (Fig. 8A, 8B & 8D). However, there were significantly more TUNEL positive pyramidal cells in mTOR$^{Cx3cr1\text{-}cre}$CKO mice at days 3 and 7 post SE compared to the controls. Concurrent with increased levels of TUNEL positive neurons at days 3 and 7 post SE, microglia proliferation was reduced in mTOR$^{Cx3cr1\text{-}cre}$CKO mice (Fig. 3A, 3B, 3E, 8D & 8E). TUNEL positivity is an indirect indicator of apoptotic cell death whereas cleaved-Caspase 3 staining is a more relevant marker of apoptosis. We found that cleaved-Caspase 3 staining was largely negative in the pyramidal layers, except for very weak staining on day 7 in mTOR$^{Cx3cr1\text{-}cre}$CKO mice (Fig. 8A, 8B & 8D). We next evaluated the density of neurons in the hippocampal CA1 region 20 days post-SE. As expected, SE caused loss of pyramidal neurons in control mice and a significant reduction in mTOR$^{Cx3cr1\text{-}cre}$CKO mice (Fig. 8C & 8F). These data suggest that microglial mTOR deletion increases neuronal loss.

Microglial mTOR deletion promotes epileptogenesis

JNeurosci Accepted Manuscript

To evaluate the impact of microglial mTOR deletion on epileptogenesis, epidural electrodes were implanted one-week post-SE. Seizure activities were recorded continuously beginning two weeks post-SE for two months (Fig. 9A & 9B). We recorded 24 mTOR$^{Cx3cr1\text{-}cre}$CKO mice and 33 littermate controls that experienced SE for 4 h. We found that 84.8% of the control animals developed spontaneous recurrent seizures (SRS) versus 100% of the mTOR$^{Cx3cr1\text{-}cre}$CKO animals (Fig. 9C); the difference is statistically significant. The duration of seizures was prolonged in mTOR$^{Cx3cr1\text{-}cre}$CKO mice compared to control mice (Fig. 9D). Furthermore, mTOR$^{Cx3cr1\text{-}cre}$CKO mice experienced more frequent seizures than control mice (Fig. 9E). We also recorded 8 mTOR$^{Cx3cr1\text{-}cre}$CKO and 13 control mice that had not been treated with pilocarpine. None of them developed SRS. Together, our data suggest that microglial mTOR deletion exacerbates the development of spontaneous seizures.

Discussion

In the present study, we revealed that mTOR-deficient microglia are less responsive to excitatory injury compared to wild-type microglia. However, microglial mTOR-deficient mice displayed a significant increase of neuronal loss and developed much more severe spontaneous seizures, suggesting a protective role of microglial mTOR in mitigating neuronal loss and attenuating epileptogenesis to excitatory injury.

mTOR-deficient microglia have a defective proliferative response to excitatory injury

Despite the presence of severe hippocampal pyramidal neuronal injuries, mTOR-deficient microglia did not hyper-proliferate in the injured pyramidal layers. Thus, the response of mTOR-deficient microglia to excitatory injury was substantially muted. Previous studies reported that microglial proliferation is inhibited by rapamycin (Brewster et al., 2013; Nguyen et al., 2015; van Vliet et al., 2016). However, it was unclear from those studies whether rapamycin acts directly on microglia or indirectly through neurons or astrocytes. Our data suggest that inhibition of microglial mTOR is sufficient to suppress the proliferative response to excitatory injury. A recent study revealed that microglial deletion of raptor, a key component in the mTORC1 complex, reduces Iba1+ cells in a focal ischemia model (Li et al., 2016), consistent with our finding of a critical role for mTOR in the proliferative response of microglia to excitatory injury. Mechanistically, it is unclear how mTOR inactivation leads to a significant loss of the proliferative response of microglia to excitatory injury. mTORC1 complex regulates cell growth,

JNeurosci Accepted Manuscript

569 which could explain the reduced length of the microglial processes we observed. As microglial
570 processes are moderately shortened in mTOR-deficient microglia, this could limit their contacts
571 with neurons and compromise their ability to detect injuries. However, we found that microglia
572 density is not significantly reduced within and around the hippocampal pyramidal layer. These
573 data suggest that, instead of there being reduced physical contacts with neurons per se, some
574 other mechanism(s) for injury detection is perhaps compromised in mTOR-deficient microglia.
575 For example, microglial phagocytosis activity is severely impaired. It is conceivable that
576 phagocytosis of cell debris released from dead or dying neurons may be necessary for microglia
577 to acquire a reactive phenotype. Recent studies revealed that some receptors regulate the
578 microglial response to excitatory injuries following SE. Down-regulation of colony-stimulating
579 factor-1 activity attenuates microglial proliferation after seizures or appears to be anti-epileptic
580 (Feng et al., 2019; Srivastava et al., 2018). Microglial P2Y12 receptors also regulate the
581 interaction of microglia and neurons (Eyo et al., 2014; Mo et al., 2019). It will be interesting to
582 see if either the expression or activation of these receptors is changed in mTOR$^{Cx3cr1\text{-}cre}$CKO
583 mice and determine if these changes are responsible for the altered microglial response to
584 excitatory injures. Apart from the lack of proliferative response, mTOR-deficient microglia could
585 be more susceptible to dying after SE in the mTOR$^{Cx3cr1\text{-}cre}$CKO mice, resulting in a reduced
586 density of microglia. Akt is a key component of mTORC2 signaling which is relatively
587 rapamycin-insensitive, but still inhibited at higher concentrations of rapamycin (Foster and
588 Toschi, 2009; Sarbassov et al., 2005). Akt plays a critical role in cell proliferation and survival
589 (Luo et al., 2003). Future study will determine if microglial viability is reduced as a result of
590 deficiency in mTOR/Akt signaling.
591
592 **mTOR deficiency impairs microglial phagocytosis**
593 Microglia are professional phagocytes in the CNS. They play an important role in modifying
594 neuronal circuits during development as well as in epilepsy, by phagocytosis of synapses and
595 neurons (Abiega et al., 2016; Brown and Neher, 2014; Hammond et al., 2018; Paolicelli et al.,
596 2011; Schafer et al., 2012; Schartz et al., 2018; Sierra et al., 2013; Wyatt-Johnson and
597 Brewster, 2020; Wyatt et al., 2017). We found that one of the major phenotypic changes in
598 mTOR-deficient microglia is the loss of ability to engulf injured neurons as well as a bacterial
599 mimetic (Zymosan) (Preissler et al., 2015). Mechanistically, mTOR signaling has been
600 implicated in microglial phagocytosis (Shen et al., 2016). In addition, several other signaling
601 pathways, i.e. complement C1q-C3 signaling, expression of P2Y12 receptors, fractalkine
602 signaling, and release of ATP, have been reported to be up-regulated following SE (Abiega et

JNeurosci Accepted Manuscript

al., 2016; Eyo et al., 2018; Eyo et al., 2016; Eyo et al., 2014; Schartz et al., 2018). It will be interesting to see if these signaling pathways are altered, resulting in impaired microglial phagocytosis in mTOR$^{Cx3cr1\text{-}cre}$CKO mice. In addition, mTOR signaling regulates the cytoskeleton and related small G-protein activity (Larson et al., 2010; Sarbassov et al., 2004), which play a critical role in regulating cell migration and phagocytosis. This could be one of the mechanisms underlying impaired phagocytosis. Although phagocytosis activity in mTOR-deficient microglia is impaired, we did not see a significant change of synapse density in mTOR$^{Cx3cr1\text{-}cre}$CKO mice. A possible explanation is that engulfment of dying neurons may involve mechanisms that could be different from synapse pruning in the unperturbed brain, which perhaps reflects the difference in "find-me, eat-me, digest-me, and don't-eat-me" signaling (Wyatt-Johnson and Brewster, 2020). Quantifying phagocytotic cups was used as a means to evaluate *in vivo* phagocytosis activity. We acknowledge that some of the phagocytotic cups could be microglia wrapping around injured neurons, but not necessarily reflecting complete phagocytosis per se.

mTOR deficiency reduces the microglial inflammatory response

mTOR deficiency reduces induction of the proinflammatory cytokines TNFα and IL-1β in microglia. Mechanistically, reduced induction of proinflammatory cytokines appears to echo low expression of the microglial activation marker CD68 in mTOR$^{Cx3cr1\text{-}cre}$CKO mice. It is conceivable that the attenuated proinflammatory response observed in microglia of mTOR$^{Cx3cr1\text{-}cre}$CKO mice is due to an intrinsic change of the inflammatory pathway in microglia as a result of mTOR deficiency or to curtailed exposure of microglia to inflammatory stimuli elicited by excitatory injuries, i.e. reduced contact or compromised phagocytosis of dead/dying neurons. Interestingly, microglial mTOR deficiency increases induction of IL-6 in non-microglial cells. The exact source of IL-6 induction and its biological significance needs to be clarified in future studies.

Microglial mTOR deficiency exacerbates neuronal loss

We observed a significant increase in loss of neurons following SE in mTOR$^{Cx3cr1\text{-}cre}$CKO mice. However, mTOR inhibition by rapamycin was reported to attenuate the neuronal loss (van Vliet et al., 2012; Zeng et al., 2009). Several factors could contribute to these disparate outcomes. Rapamycin could inhibit mTOR in both neurons and microglia, whereas in our study mTOR activity was restrictively removed in microglia. In addition, mTOR$^{Cx3cr1\text{-}cre}$CKO mice became more susceptible to SE compared to their littermate controls. We cannot rule out the possibility that severe seizures in mTOR$^{Cx3cr1\text{-}cre}$CKO mice could account for the increased excitatory

JNeurosci Accepted Manuscript

injury, leading to greater loss of neurons. However, in the present study, both control and mTOR$^{Cx3cr1\text{-}cre}$CKO mice were subjected to careful dosing and experienced similar levels of SE. Also, the levels of initial excitatory injury were comparable based on FJB and TUNEL staining at day 1 post-SE, but a significant increase in TUNEL staining was observed at days 3 and 7 post-SE in the mTOR$^{Cx3cr1\text{-}cre}$CKO mice, indicating that neuronal injury continues to exacerbate even 24 hours after the initial excitatory injury, becoming more severe in mTOR$^{Cx3cr1\text{-}cre}$CKO mice than in control mice. At the same time, proliferation and activation of microglia were significantly muted in mTOR$^{Cx3cr1\text{-}cre}$CKO mice. It is conceivable that engulfing or wrapping around the dying neurons prior to their lysis could be key to effectively contain the propagation of excitatory damage, thereby better maintaining CNS homeostasis. Compromised microglial phagocytosis could also lead to accumulation of dying neurons in mTOR$^{Cx3cr1\text{-}cre}$CKO mice. A previous study reported that pharmacological inhibition of microglial proliferation by a colony-stimulating factor-1 inhibitor saves neurons from excitatory toxicity (Feng et al., 2019). In the present study, neuronal loss was exacerbated in mTOR$^{Cx3cr1\text{-}cre}$CKO mice in which microglial proliferation was significantly muted. The discrepancy could reflect involvement of different signaling pathways, resulting in opposite effects. While apoptotic neuronal death has long been reported in excitatory loss in epilepsy, we did not see any increase of cleaved caspase-3 staining, nor any increase of cleaved caspase-3 by western blot analysis (data not shown). Our observation is in line with previous studies that cleaved caspase-3 is nearly undetectable in the pilocarpine model (Varvel et al., 2016) and its positivity is less than 10% in TUNEL positive neurons in a kainate model (Araki et al., 2002). All these studies suggest that pyramidal cell death may involve mechanisms other than classic apoptosis (Dingledine et al., 2014). SE triggers a significant infiltration of Cx3cr1^{+} monocytes into the brain, despite the fact that resident microglia are mainly proliferated in the hippocampus (Feng et al., 2019; Tian et al., 2017; Varvel et al., 2016). We acknowledge that the overall effect could be a mix of inputs from both microglia and macrophages.

A counterintuitive role of microglial mTOR in epileptogenesis of acquired epilepsy

Studies over the past decade have brought compelling evidence that aberrant activation of the mTOR pathway is strongly epileptogenic. Gain-of-function mutations, due either to inherited mutation or to somatic mutation, account for the abnormal brain development which forms the basis of genetic epilepsy in humans (Crino, 2016; D'Gama et al., 2015; Jansen et al., 2015; Talos et al., 2018; Wong, 2013). Modeling hyper-activation of mTOR either in neurons or glial cells in various animal models is also epileptogenic (Carson et al., 2012; Feliciano et al., 2011;

JNeurosci Accepted Manuscript

McMahon et al., 2012; Meikle et al., 2007; Orlova et al., 2010; Sunnen et al., 2011; Uhlmann et al., 2002; Zhang et al., 2016; Zhao et al., 2018). In addition, the mTOR inhibitor rapamycin attenuates the development of epilepsy, reduces seizure frequency, and suppresses mossy fiber sprouting (Buckmaster et al., 2009; Huang et al., 2012; Raffo et al., 2011; Sunnen et al., 2011; Talos et al., 2012; Zeng et al., 2009). However, the effect of rapamycin is not always consistent (Buckmaster et al., 2009; Gericke et al., 2019; Zeng et al., 2009). The broad presence of mTOR signaling in brain cells could prevent mTOR inhibitors from achieving a net therapeutic effect. Notably, previous studies have focused on gain-of-function mTOR mutations, so it will be interesting to determine the impact of loss-of-function mTOR mutations in epilepsy.

While microglial-specific inactivation of mTOR activity provides a much finer granularity of mTOR signaling in epileptogenesis, genetic approaches also have some inherent limitations, such as a change in baseline. In the present study, we did not employ the Cx3cr1-CreER inducible line because this line has spontaneous leakage in microglia prior to tamoxifen treatment (Zhang et al., 2018; Zhao et al., 2018; Zhao et al., 2019). Microglial deletion of mTOR causes a moderate increase of seizure susceptibility to pilocarpine. Therefore, we carefully performed pilocarpine dosing so as to induce comparable levels of initial excitatory injuries between control and $mTOR^{Cx3cr1\text{-}cre}CKO$ mice. We acknowledge that, apart from an epileptogenic role of the muted response of mTOR-deficient microglia to excitatory injury, we cannot rule out a contribution from changes to neurons as a result of microglial mTOR deletion. However, both possibilities point to the same conclusion, that deficiency of mTOR signaling in microglia increases seizure susceptibility.

In summary, our study revealed that activation of microglial mTOR is neuronal protective and anti-epileptogenic in an acquired epilepsy model. Our finding is a significant departure from the prevailing tenet that excessive activation of mTOR is epileptogenic and explains why the effect of rapamycin is not consistent or even paradoxical in previous studies. The results from our study could better guide the use of rapamycin in treating or preventing epilepsy.

References:

Abiega, O., Beccari, S., Diaz-Aparicio, I., Nadjar, A., Laye, S., Leyrolle, Q., Gomez-Nicola, D., Domercq, M., Perez-Samartin, A., Sanchez-Zafra, V.*, et al.* (2016). Neuronal Hyperactivity Disturbs ATP Microgradients, Impairs Microglial Motility, and Reduces Phagocytic Receptor Expression Triggering Apoptosis/Microglial Phagocytosis Uncoupling. PLoS Biol *14*, e1002466.

JNeurosci Accepted Manuscript

Abraham, J., Fox, P.D., Condello, C., Bartolini, A., and Koh, S. (2012). Minocycline attenuates microglia activation and blocks the long-term epileptogenic effects of early-life seizures. Neurobiol Dis *46*, 425-430.

Araki, T., Simon, R.P., Taki, W., Lan, J.Q., and Henshall, D.C. (2002). Characterization of neuronal death induced by focally evoked limbic seizures in the C57BL/6 mouse. J Neurosci Res *69*, 614-621.

Aronica, E., Bauer, S., Bozzi, Y., Caleo, M., Dingledine, R., Gorter, J.A., Henshall, D.C., Kaufer, D., Koh, S., Loscher, W*., et al.* (2017). Neuroinflammatory targets and treatments for epilepsy validated in experimental models. Epilepsia *58 Suppl 3*, 27-38.

Beach, T.G., Woodhurst, W.B., MacDonald, D.B., and Jones, M.W. (1995). Reactive microglia in hippocampal sclerosis associated with human temporal lobe epilepsy. Neurosci Lett *191*, 27-30.

Boer, K., Spliet, W.G., van Rijen, P.C., Redeker, S., Troost, D., and Aronica, E. (2006). Evidence of activated microglia in focal cortical dysplasia. J Neuroimmunol *173*, 188-195.

Boer, K., Troost, D., Jansen, F., Nellist, M., van den Ouweland, A.M., Geurts, J.J., Spliet, W.G., Crino, P., and Aronica, E. (2008). Clinicopathological and immunohistochemical findings in an autopsy case of tuberous sclerosis complex. Neuropathology *28*, 577-590.

Borges, K., Gearing, M., McDermott, D.L., Smith, A.B., Almonte, A.G., Wainer, B.H., and Dingledine, R. (2003). Neuronal and glial pathological changes during epileptogenesis in the mouse pilocarpine model. Exp Neurol *182*, 21-34.

Brewster, A.L., Lugo, J.N., Patil, V.V., Lee, W.L., Qian, Y., Vanegas, F., and Anderson, A.E. (2013). Rapamycin reverses status epilepticus-induced memory deficits and dendritic damage. PLoS One *8*, e57808.

Brown, G.C., and Neher, J.J. (2014). Microglial phagocytosis of live neurons. Nat Rev Neurosci *15*, 209-216.

Buckmaster, P.S., Ingram, E.A., and Wen, X. (2009). Inhibition of the mammalian target of rapamycin signaling pathway suppresses dentate granule cell axon sprouting in a rodent model of temporal lobe epilepsy. J Neurosci *29*, 8259-8269.

Carson, R.P., Van Nielen, D.L., Winzenburger, P.A., and Ess, K.C. (2012). Neuronal and glia abnormalities in Tsc1-deficient forebrain and partial rescue by rapamycin. Neurobiol Dis *45*, 369-380.

Crino, P.B. (2016). The mTOR signalling cascade: paving new roads to cure neurological disease. Nat Rev Neurol *12*, 379-392.

D'Gama, A.M., Geng, Y., Couto, J.A., Martin, B., Boyle, E.A., LaCoursiere, C.M., Hossain, A., Hatem, N.E., Barry, B.J., Kwiatkowski, D.J*., et al.* (2015). Mammalian target of rapamycin pathway mutations cause hemimegalencephaly and focal cortical dysplasia. Ann Neurol *77*, 720-725.

JNeurosci Accepted Manuscript

Dingledine, R., Varvel, N.H., and Dudek, F.E. (2014). When and how do seizures kill neurons, and is cell death relevant to epileptogenesis? Adv Exp Med Biol *813*, 109-122.

Eyo, U.B., Mo, M., Yi, M.H., Murugan, M., Liu, J., Yarlagadda, R., Margolis, D.J., Xu, P., and Wu, L.J. (2018). P2Y12R-Dependent Translocation Mechanisms Gate the Changing Microglial Landscape. Cell Rep *23*, 959-966.

Eyo, U.B., Peng, J., Murugan, M., Mo, M., Lalani, A., Xie, P., Xu, P., Margolis, D.J., and Wu, L.J. (2016). Regulation of Physical Microglia-Neuron Interactions by Fractalkine Signaling after Status Epilepticus. eNeuro *3*.

Eyo, U.B., Peng, J., Swiatkowski, P., Mukherjee, A., Bispo, A., and Wu, L.J. (2014). Neuronal hyperactivity recruits microglial processes via neuronal NMDA receptors and microglial P2Y12 receptors after status epilepticus. J Neurosci *34*, 10528-10540.

Feliciano, D.M., Su, T., Lopez, J., Platel, J.C., and Bordey, A. (2011). Single-cell Tsc1 knockout during corticogenesis generates tuber-like lesions and reduces seizure threshold in mice. J Clin Invest *121*, 1596-1607.

Feng, L., Murugan, M., Bosco, D.B., Liu, Y., Peng, J., Worrell, G.A., Wang, H.L., Ta, L.E., Richardson, J.R., Shen, Y.*, et al.* (2019). Microglial proliferation and monocyte infiltration contribute to microgliosis following status epilepticus. Glia *67*, 1434-1448.

Foster, D.A., and Toschi, A. (2009). Targeting mTOR with rapamycin: one dose does not fit all. Cell Cycle *8*, 1026-1029.

Gericke, B., Brandt, C., Theilmann, W., Welzel, L., Schidlitzki, A., Twele, F., Kaczmarek, E., Anjum, M., Hillmann, P., and Loscher, W. (2019). Selective inhibition of mTORC1/2 or PI3K/mTORC1/2 signaling does not prevent or modify epilepsy in the intrahippocampal kainate mouse model. Neuropharmacology *162*, 107817.

Hammond, T.R., Robinton, D., and Stevens, B. (2018). Microglia and the Brain: Complementary Partners in Development and Disease. Annu Rev Cell Dev Biol *34*, 523-544.

Huang, X., McMahon, J., Yang, J., Shin, D., and Huang, Y. (2012). Rapamycin down-regulates KCC2 expression and increases seizure susceptibility to convulsants in immature rats. Neuroscience *219*, 33-47.

Huang, X., Zhang, H., Yang, J., Wu, J., McMahon, J., Lin, Y., Cao, Z., Gruenthal, M., and Huang, Y. (2010). Pharmacological inhibition of the mammalian target of rapamycin pathway suppresses acquired epilepsy. Neurobiol Dis *40*, 193-199.

Jansen, L.A., Mirzaa, G.M., Ishak, G.E., O'Roak, B.J., Hiatt, J.B., Roden, W.H., Gunter, S.A., Christian, S.L., Collins, S., Adams, C.*, et al.* (2015). PI3K/AKT pathway mutations cause a spectrum of brain malformations from megalencephaly to focal cortical dysplasia. Brain *138*, 1613-1628.

Kassai, H., Sugaya, Y., Noda, S., Nakao, K., Maeda, T., Kano, M., and Aiba, A. (2014). Selective activation of mTORC1 signaling recapitulates microcephaly, tuberous sclerosis, and neurodegenerative diseases. Cell Rep *7*, 1626-1639.

JNeurosci Accepted Manuscript

Larson, Y., Liu, J., Stevens, P.D., Li, X., Li, J., Evers, B.M., and Gao, T. (2010). Tuberous sclerosis complex 2 (TSC2) regulates cell migration and polarity through activation of CDC42 and RAC1. J Biol Chem *285*, 24987-24998.

Li, D., Wang, C., Yao, Y., Chen, L., Liu, G., Zhang, R., Liu, Q., Shi, F.D., and Hao, J. (2016). mTORC1 pathway disruption ameliorates brain inflammation following stroke via a shift in microglia phenotype from M1 type to M2 type. FASEB J *30*, 3388-3399.

Liddelow, S.A., Guttenplan, K.A., Clarke, L.E., Bennett, F.C., Bohlen, C.J., Schirmer, L., Bennett, M.L., Munch, A.E., Chung, W.S., Peterson, T.C.*, et al.* (2017). Neurotoxic reactive astrocytes are induced by activated microglia. Nature *541*, 481-487.

Liu, J., Reeves, C., Michalak, Z., Coppola, A., Diehl, B., Sisodiya, S.M., and Thom, M. (2014). Evidence for mTOR pathway activation in a spectrum of epilepsy-associated pathologies. Acta Neuropathol Commun *2*, 71.

Luo, H.R., Hattori, H., Hossain, M.A., Hester, L., Huang, Y., Lee-Kwon, W., Donowitz, M., Nagata, E., and Snyder, S.H. (2003). Akt as a mediator of cell death. Proc Natl Acad Sci U S A *100*, 11712-11717.

McMahon, J., Huang, X., Yang, J., Komatsu, M., Yue, Z., Qian, J., Zhu, X., and Huang, Y. (2012). Impaired autophagy in neurons after disinhibition of mammalian target of rapamycin and its contribution to epileptogenesis. J Neurosci *32*, 15704-15714.

Meikle, L., Talos, D.M., Onda, H., Pollizzi, K., Rotenberg, A., Sahin, M., Jensen, F.E., and Kwiatkowski, D.J. (2007). A mouse model of tuberous sclerosis: neuronal loss of Tsc1 causes dysplastic and ectopic neurons, reduced myelination, seizure activity, and limited survival. J Neurosci *27*, 5546-5558.

Miron, V.E. (2017). Microglia-driven regulation of oligodendrocyte lineage cells, myelination, and remyelination. J Leukoc Biol *101*, 1103-1108.

Mo, M., Eyo, U.B., Xie, M., Peng, J., Bosco, D.B., Umpierre, A.D., Zhu, X., Tian, D.S., Xu, P., and Wu, L.J. (2019). Microglial P2Y12 Receptor Regulates Seizure-Induced Neurogenesis and Immature Neuronal Projections. J Neurosci *39*, 9453-9464.

Nguyen, L.H., Brewster, A.L., Clark, M.E., Regnier-Golanov, A., Sunnen, C.N., Patil, V.V., D'Arcangelo, G., and Anderson, A.E. (2015). mTOR inhibition suppresses established epilepsy in a mouse model of cortical dysplasia. Epilepsia *56*, 636-646.

Nguyen, L.H., Mahadeo, T., and Bordey, A. (2019). mTOR Hyperactivity Levels Influence the Severity of Epilepsy and Associated Neuropathology in an Experimental Model of Tuberous Sclerosis Complex and Focal Cortical Dysplasia. J Neurosci *39*, 2762-2773.

Nimmerjahn, A., Kirchhoff, F., and Helmchen, F. (2005). Resting microglial cells are highly dynamic surveillants of brain parenchyma in vivo. Science *308*, 1314-1318.

Nonoda, Y., Saito, Y., Itoh, M., Nakagawa, E., Sugai, K., Takahashi, A., Otsuki, T., Saito, Y., Arima, K., Mizuguchi, M.*, et al.* (2009). Activation of microglia/macrophages expressing phosphorylated S6 ribosomal protein in a case of hemimegalencephaly with progressive calcification and atrophy. J Neurol Sci *287*, 52-59.

JNeurosci Accepted Manuscript

Orlova, K.A., Parker, W.E., Heuer, G.G., Tsai, V., Yoon, J., Baybis, M., Fenning, R.S., Strauss, K., and Crino, P.B. (2010). STRADalpha deficiency results in aberrant mTORC1 signaling during corticogenesis in humans and mice. J Clin Invest *120*, 1591-1602.

Paolicelli, R.C., Bolasco, G., Pagani, F., Maggi, L., Scianni, M., Panzanelli, P., Giustetto, M., Ferreira, T.A., Guiducci, E., Dumas, L.*, et al.* (2011). Synaptic pruning by microglia is necessary for normal brain development. Science *333*, 1456-1458.

Preissler, J., Grosche, A., Lede, V., Le Duc, D., Krugel, K., Matyash, V., Szulzewsky, F., Kallendrusch, S., Immig, K., Kettenmann, H.*, et al.* (2015). Altered microglial phagocytosis in GPR34-deficient mice. Glia *63*, 206-215.

Quan, Y., Jiang, J., and Dingledine, R. (2013). EP2 receptor signaling pathways regulate classical activation of microglia. J Biol Chem *288*, 9293-9302.

Racine, R.J. (1972). Modification of seizure activity by electrical stimulation. II. Motor seizure. Electroencephalogr Clin Neurophysiol *32*, 281-294.

Raffo, E., Coppola, A., Ono, T., Briggs, S.W., and Galanopoulou, A.S. (2011). A pulse rapamycin therapy for infantile spasms and associated cognitive decline. Neurobiol Dis *43*, 322-329.

Sarbassov, D.D., Ali, S.M., Kim, D.H., Guertin, D.A., Latek, R.R., Erdjument-Bromage, H., Tempst, P., and Sabatini, D.M. (2004). Rictor, a novel binding partner of mTOR, defines a rapamycin-insensitive and raptor-independent pathway that regulates the cytoskeleton. Curr Biol *14*, 1296-1302.

Sarbassov, D.D., Guertin, D.A., Ali, S.M., and Sabatini, D.M. (2005). Phosphorylation and regulation of Akt/PKB by the rictor-mTOR complex. Science *307*, 1098-1101.

Schafer, D.P., Lehrman, E.K., Kautzman, A.G., Koyama, R., Mardinly, A.R., Yamasaki, R., Ransohoff, R.M., Greenberg, M.E., Barres, B.A., and Stevens, B. (2012). Microglia sculpt postnatal neural circuits in an activity and complement-dependent manner. Neuron *74*, 691-705.

Schartz, N.D., Wyatt-Johnson, S.K., Price, L.R., Colin, S.A., and Brewster, A.L. (2018). Status epilepticus triggers long-lasting activation of complement C1q-C3 signaling in the hippocampus that correlates with seizure frequency in experimental epilepsy. Neurobiol Dis *109*, 163-173.

Shen, K., Sidik, H., and Talbot, W.S. (2016). The Rag-Ragulator Complex Regulates Lysosome Function and Phagocytic Flux in Microglia. Cell Rep *14*, 547-559.

Shibuya, Y., Chang, C.C., Huang, L.H., Bryleva, E.Y., and Chang, T.Y. (2014). Inhibiting ACAT1/SOAT1 in microglia stimulates autophagy-mediated lysosomal proteolysis and increases Abeta1-42 clearance. J Neurosci *34*, 14484-14501.

Sierra, A., Abiega, O., Shahraz, A., and Neumann, H. (2013). Janus-faced microglia: beneficial and detrimental consequences of microglial phagocytosis. Front Cell Neurosci *7*, 6.

JNeurosci Accepted Manuscript

908 Sierra, A., Encinas, J.M., Deudero, J.J., Chancey, J.H., Enikolopov, G., Overstreet-Wadiche,
909 L.S., Tsirka, S.E., and Maletic-Savatic, M. (2010). Microglia shape adult hippocampal
910 neurogenesis through apoptosis-coupled phagocytosis. Cell Stem Cell *7*, 483-495.
911
912 Sosunov, A.A., Wu, X., McGovern, R.A., Coughlin, D.G., Mikell, C.B., Goodman, R.R., and
913 McKhann, G.M., 2nd (2012). The mTOR pathway is activated in glial cells in mesial temporal
914 sclerosis. Epilepsia *53 Suppl 1*, 78-86.
915
916 Srivastava, P.K., van Eyll, J., Godard, P., Mazzuferi, M., Delahaye-Duriez, A., Van
917 Steenwinckel, J., Gressens, P., Danis, B., Vandenplas, C., Foerch, P.*, et al.* (2018). A systems-
918 level framework for drug discovery identifies Csf1R as an anti-epileptic drug target. Nat
919 Commun *9*, 3561.
920
921 Sunnen, C.N., Brewster, A.L., Lugo, J.N., Vanegas, F., Turcios, E., Mukhi, S., Parghi, D.,
922 D'Arcangelo, G., and Anderson, A.E. (2011). Inhibition of the mammalian target of rapamycin
923 blocks epilepsy progression in NS-Pten conditional knockout mice. Epilepsia *52*, 2065-2075.
924
925 Talos, D.M., Jacobs, L.M., Gourmaud, S., Coto, C.A., Sun, H., Lim, K.C., Lucas, T.H., Davis,
926 K.A., Martinez-Lage, M., and Jensen, F.E. (2018). Mechanistic target of rapamycin complex 1
927 and 2 in human temporal lobe epilepsy. Ann Neurol *83*, 311-327.
928
929 Talos, D.M., Sun, H., Zhou, X., Fitzgerald, E.C., Jackson, M.C., Klein, P.M., Lan, V.J., Joseph,
930 A., and Jensen, F.E. (2012). The interaction between early life epilepsy and autistic-like
931 behavioral consequences: a role for the mammalian target of rapamycin (mTOR) pathway.
932 PLoS One *7*, e35885.
933
934 Tian, D.S., Peng, J., Murugan, M., Feng, L.J., Liu, J.L., Eyo, U.B., Zhou, L.J., Mogilevsky, R.,
935 Wang, W., and Wu, L.J. (2017). Chemokine CCL2-CCR2 Signaling Induces Neuronal Cell
936 Death via STAT3 Activation and IL-1beta Production after Status Epilepticus. J Neurosci *37*,
937 7878-7892.
938
939 Uhlmann, E.J., Wong, M., Baldwin, R.L., Bajenaru, M.L., Onda, H., Kwiatkowski, D.J., Yamada,
940 K., and Gutmann, D.H. (2002). Astrocyte-specific TSC1 conditional knockout mice exhibit
941 abnormal neuronal organization and seizures. Ann Neurol *52*, 285-296.
942
943 van Vliet, E.A., Forte, G., Holtman, L., den Burger, J.C., Sinjewel, A., de Vries, H.E., Aronica, E.,
944 and Gorter, J.A. (2012). Inhibition of mammalian target of rapamycin reduces epileptogenesis
945 and blood-brain barrier leakage but not microglia activation. Epilepsia *53*, 1254-1263.
946
947 van Vliet, E.A., Otte, W.M., Wadman, W.J., Aronica, E., Kooij, G., de Vries, H.E., Dijkhuizen,
948 R.M., and Gorter, J.A. (2016). Blood-brain barrier leakage after status epilepticus in rapamycin-
949 treated rats II: Potential mechanisms. Epilepsia *57*, 70-78.
950
951 Varvel, N.H., Neher, J.J., Bosch, A., Wang, W., Ransohoff, R.M., Miller, R.J., and Dingledine, R.
952 (2016). Infiltrating monocytes promote brain inflammation and exacerbate neuronal damage
953 after status epilepticus. Proc Natl Acad Sci U S A *113*, E5665-5674.
954
955 Vezzani, A., and Viviani, B. (2015). Neuromodulatory properties of inflammatory cytokines and
956 their impact on neuronal excitability. Neuropharmacology *96*, 70-82.
957

JNeurosci Accepted Manuscript

Wlodarczyk, A., Holtman, I.R., Krueger, M., Yogev, N., Bruttger, J., Khorooshi, R., Benmamar-Badel, A., de Boer-Bergsma, J.J., Martin, N.A., Karram, K.*, et al.* (2017). A novel microglial subset plays a key role in myelinogenesis in developing brain. EMBO J *36*, 3292-3308.

Wolf, S.A., Boddeke, H.W., and Kettenmann, H. (2017). Microglia in Physiology and Disease. Annu Rev Physiol *79*, 619-643.

Wong, M. (2013). A critical review of mTOR inhibitors and epilepsy: from basic science to clinical trials. Expert Rev Neurother *13*, 657-669.

Wyatt-Johnson, S.K., and Brewster, A.L. (2020). Emerging Roles for Microglial Phagocytic Signaling in Epilepsy. Epilepsy Curr *20*, 33-38.

Wyatt, S.K., Witt, T., Barbaro, N.M., Cohen-Gadol, A.A., and Brewster, A.L. (2017). Enhanced classical complement pathway activation and altered phagocytosis signaling molecules in human epilepsy. Exp Neurol *295*, 184-193.

Zeng, L.H., Rensing, N.R., and Wong, M. (2009). The mammalian target of rapamycin signaling pathway mediates epileptogenesis in a model of temporal lobe epilepsy. J Neurosci *29*, 6964-6972.

Zhang, B., Zou, J., Han, L., Beeler, B., Friedman, J.L., Griffin, E., Piao, Y.S., Rensing, N.R., and Wong, M. (2018). The specificity and role of microglia in epileptogenesis in mouse models of tuberous sclerosis complex. Epilepsia *59*, 1796-1806.

Zhang, B., Zou, J., Han, L., Rensing, N., and Wong, M. (2016). Microglial activation during epileptogenesis in a mouse model of tuberous sclerosis complex. Epilepsia *57*, 1317-1325.

Zhao, X., Liao, Y., Morgan, S., Mathur, R., Feustel, P., Mazurkiewicz, J., Qian, J., Chang, J., Mathern, G.W., Adamo, M.A.*, et al.* (2018). Noninflammatory Changes of Microglia Are Sufficient to Cause Epilepsy. Cell Rep *22*, 2080-2093.

Zhao, X.F., Alam, M.M., Liao, Y., Huang, T., Mathur, R., Zhu, X., and Huang, Y. (2019). Targeting Microglia Using Cx3cr1-Cre Lines: Revisiting the Specificity. eNeuro *6*.

JNeurosci Accepted Manuscript

Figure legends

Fig. 1 Activation of mTOR in microglia following status epilepticus (SE)

A. Confocal images acquired from cortex (CTX), hippocampus CA1 and CA3, and the dentate gyrus (DG). Scale bar, 20 μm. B & C: Quantification of p-S6/Iba1 double positive microglial cells (B) and CD68/Iba1 double positive microglial cells (C) in sham-treated (n=4; 2 males and 2 females), SE-3d (n=5; 2 males and 3 females) and SE-3d+Rapamycin (n=4; 2 males and 2 females) mice. Data are presented as mean ± SEM. Sample comparison was made among three groups (Sham, SE and SE + rapamycin groups) and analyzed with one-way ANOVA (P1), followed by Tukey's multiple comparisons test (P2: comparison between control and SE; P3: between SE and SE + Rapamycin).

Fig. 2 Characterization of microglial morphology in *mTOR*$^{Cx3cr1\text{-}cre}$CKO mice

A. Brain coronal sections from control and *mTOR*$^{Cx3cr1\text{-}cre}$CKO mice were stained with anti-Iba1 (green) and DAPI (blue). Representative images with entire cortical and hippocampal fields and high magnification of images from CTX and CA1. Scale bar: 200 μm (whole scale), 20 μm (ROI).

B) Confocal images (green + blue) and Imaris three-dimensional reconstructed images (cyan) from CTX, CA1, CA3 and DG of control and *mTOR*$^{Cx3cr1\text{-}cre}$CKO mice. Scale bar, 20 μm.

C) Imaris-based automatic quantification of microglial cell volume, dendrite length, number of branch points, number of terminal points, and number of segments in control (n=5; 2 males and 3 females) and *mTOR*$^{Cx3cr1\text{-}cre}$CKO mice (n=4; 2 males and 2 females). Data are presented as mean ± SEM. A two-tailed unpaired *t* test was used for the comparison between control and *mTOR*^{Cx3cr1}CKO mice.

Fig. 3 Microglial proliferation and activation in control and *mTOR*$^{Cx3cr1\text{-}cre}$CKO mice following SE

A. Full montage of confocal images showing acute injury (FJB+, green), microglial density (Iba1+, green), and CD68 expression (CD68+, red) in the hippocampus of control and *mTOR*$^{Cx3cr1\text{-}cre}$CKO mice either sham-treated or 1-7 days post-SE. Scale bar, 200 μm.

B. Representative confocal images acquired from the CA1 of control and *mTOR*$^{Cx3cr1\text{-}cre}$CKO mice either sham-treated or 1-7 days post-SE. Scale bar, 20 μm.

C. Representative confocal images showing Ki67 expression (Ki67+, red) in the CA1 of control and *mTOR*$^{Cx3cr1\text{-}cre}$CKO mice either sham-treated or 1-7 days post-SE. Scale bar, 20 μm.

JNeurosci Accepted Manuscript

D. Average doses of pilocarpine that induced stage 4/5 seizures in control and *mTOR*$^{Cx3cr1\text{-}cre}$CKO mice.

E & F: Quantification of Iba1-positive microglia and CD68 immunofluorescence intensity in control and *mTOR*$^{Cx3cr1\text{-}cre}$CKO mice either sham-treated or 1-7 days post-SE. Sample sizes in control groups: Sham (n=6; 3 males and 3 females), SE-1d (n=6; 3 males and 3 females), SE-3d (n=6; 3 males and 3 females), and SE-7d (n=6; 3 males and 3 females); and in the *mTOR*$^{Cx3cr1\text{-}cre}$CKO groups: Sham (n=4; 2 males and 2 females), SE-1d (n=5; 2 males and 3 females), SE3d (n=6; 3 males and 3 females), and SE-7d (n=4; 2 males and 2 females).

G. Quantification of Ki67/Iba1 double-positive microglial cells in control and *mTOR*$^{Cx3cr1\text{-}cre}$CKO mice either sham-treated or 1-7 days post-SE. Sample sizes in control groups: Sham (n=6; 3 males and 3 females), SE-1d (n=6; 3 males and 3 females), SE-3d (n=6; 3 males and 3 females), and SE-7d (n=6; 3 males and 3 females); and in the *mTOR*$^{Cx3cr1\text{-}cre}$CKO groups: Sham (n=4; 2 males and 2 females), SE-1d (n=5; 2 males and 3 females), SE3d (n=6; 3 males and 3 females), and SE-7d (n=4; 2 males and 2 females).

Data are presented as mean ± SEM. A two-tailed unpaired *t* test was used for the comparison between control and *mTOR*^{Cx3cr1}CKO mice.

Fig. 4 mTOR deletion decreases microglial phagocytosis activity *in vivo* following SE and *in vitro* phagocytosis of zymosan bioparticles

A. Representative confocal images acquired from the CA1 of control and *mTOR*$^{Cx3cr1\text{-}cre}$CKO mice either sham-treated or 1-7 days post-SE. Microglia were labeled by Iba1 (green). Scale bar, 20 μm.

B. Representative images from *in vitro* live-imaging of microglial phagocytosis of pHrodo Green zymosan bioparticles (pHrodo+, green). Scale bar, 10 μm.

C. Quantification of microglial phagocytosis capacity in control and *mTOR*$^{Cx3cr1\text{-}cre}$CKO mice either sham-treated or 1-7 days post-SE. Sample sizes in control groups: Sham (n=6; 3 males and 3 females), SE-1d (n=6; 3 males and 3 females), SE-3d (n=6; 3 males and 3 females), and SE-7d (n=6; 3 males and 3 females); and in the *mTOR*$^{Cx3cr1\text{-}cre}$CKO groups: Sham (n=4; 2 males and 2 females), SE-1d (n=5; 2 males and 3 females), SE3d (n=6; 3 males and 3 females), and SE-7d (n=4; 2 males and 2 females).

Data are presented as mean ± SEM. A two-tailed unpaired *t* test was used for the comparison between control and *mTOR*^{Cx3cr1}CKO mice.

D. Quantification of the number of phagocytotic particles per microglial cell at each time point in cultured microglia prepared from control and *mTOR*$^{Cx3cr1\text{-}cre}$CKO mice (n=40 for each time point).

JNeurosci Accepted Manuscript

Data are presented as mean ± SEM. Two-way ANOVA, followed by Sidak test, was used for the comparison of *in vitro* phagocytosis between the control and *mTOR*^{Cx3cr1}*-creCKO* groups at each time point.

Fig. 5 Impact of microglial mTOR deletion on the inflammatory response following SE

A. qRT-PCR analysis of cytokine expression in hippocampal tissues harvested from control and *mTOR*^{Cx3cr1}CKO mice either sham-treated or 1-7 days post-SE. Sample sizes in the control groups are: Sham (n=7; 4 males and 3 females), SE-1d (n=8; 4 males and 4 females), SE-3d (n=5; 3 males and 2 females), and SE-7d (n=6; 3 males and 3 females); and in the *mTOR*^{Cx3cr1}CKO groups: Sham (n=4; 2 males and 2 females), SE-1d (n=7; 4 males and 3 females), SE-3d (n=5; 3 males and 2 females), and SE-7d (n=4; 2 males and 2 females).

B. Cytokine expression in purified microglia from control and *mTOR*^{Cx3cr1}CKO mice either sham-treated or 1-7 days post-SE. Sample sizes in the control groups are: Sham (n=9; 5 males and 4 females), SE-1d (n=8; 4 males and 4 females), SE-3d (n=7; 3 males and 4 females), and SE-7d (n=8; 4 males and 4 females); and in the *mTOR*^{Cx3cr1}CKO groups: Sham (n=4; 2 males and 2 females), SE-1d (n=4; 2 males and 2 females), SE-3d (n=4; 2 males and 2 females), and SE-7d (n=5; 2 males and 3 females). A two-tailed unpaired *t* test was used for the comparison between control and *mTOR*^{Cx3cr1}CKO mice. Data are presented as mean ± SEM.

Fig. 6 Impact of microglial mTOR deletion on astrocyte proliferation following SE

A. Full montage of confocal images showing astrocyte proliferation (GFAP+, green) in the cortex and hippocampus of control and *mTOR*$^{Cx3cr1\text{-}cre}$CKO mice either sham-treated or 1-7 days post-SE. Scale bar, 200 μm.

B. Representative confocal images acquired from the CTX and CA1 of control and *mTOR*$^{Cx3cr1\text{-}cre}$CKO mice either sham-treated or 1-7 days post-SE. Scale bar, 20 μm.

C. Quantification of GFAP-positive astrocytes in control and *mTOR*$^{Cx3cr1\text{-}cre}$CKO mice either sham-treated or 1-7 days post-SE. Sample sizes in control groups: Sham (n=6; 3 males and 3 females), SE-1d (n=6; 3 males and 3 females), SE-3d (n=6; 3 males and 3 females), and SE-7d (n=6; 3 males and 3 females); and in the *mTOR*$^{Cx3cr1\text{-}cre}$CKO groups: Sham (n=4; 2 males and 2 females), SE-1d (n=5; 2 males and 3 females), SE-3d (n=6; 3 males and 3 females), and SE-7d (n=4; 2 males and 2 females). A two-tailed unpaired *t* test was used for the comparison between control and *mTOR*^{Cx3cr1}CKO mice. Data are presented as mean ± SEM.

Fig. 7 Impact of microglial mTOR deletion on density of synapses

JNeurosci Accepted Manuscript

A) Representative super-resolution images of co-immunostaining of VGlut2 (red)/Homer1 (green) and vGAT (green)/Gephyrin (red) in the M1 motor cortex around layer IV (CTX) and the hippocampal (HIP) radiatum layer adjacent to pyramidal CA1 (CA1) of control and *mTOR*^{Cx3cr1}CKO mice. Synapses were identified as yellow dots, reflecting co-localization of the pre-synaptic markers vGlut2 and vGAT with the postsynaptic markers Homer1 and Gephyrin. Scale bar, 5 μm.

B) Quantification of the excitatory and inhibitory synapse densities in the CTX and HIP of wild-type (n = 5; 2 males and 3 females) and *mTOR*^{Cx3cr1}CKO (n = 5; 2 males and 3 females) mice. Data are presented as mean ± SEM. A two-tailed unpaired *t* test was used for the comparison between control and *mTOR*^{Cx3cr1}CKO mice.

Fig. 8 Impact of microglial mTOR deletion on neuronal loss following SE

A. Full montage of confocal images covering the entire hippocampus field showing FJB staining (FJB+, green), TUNEL staining (TUNEL+, red) and cleaved-Caspase3 expression (Cleaved-Cas3+, green) in control and *mTOR*$^{Cx3cr1\text{-}cre}$CKO mice either sham-treated or 1-7 days post-SE. Scale bar, 200 μm. Images were acquired by tiling and stitching of individual high-resolution images captured with a 40× objective lens. The overall sampling depth is 15 μm. Scale bar, 200 μm.

B. Representative confocal images acquired from the CA1 of control and *mTOR*$^{Cx3cr1\text{-}cre}$CKO mice either sham-treated or 1-7 days post-SE. Scale bar, 20 μm.

C. Representative images showing Nissl staining of control and *mTOR*$^{Cx3cr1\text{-}cre}$CKO mice either sham-treated or 20 days post-SE. Scale bar, 100 μm.

D. Quantification of TUNEL- and cleaved-Caspase3-positive cells in control and *mTOR*$^{Cx3cr1\text{-}cre}$CKO mice either sham-treated or 1-7 days post-SE. Sample sizes in control groups: Sham (n=6; 3 males and 3 females), SE-1d (n=6; 3 males and 3 females), SE-3d (n=6; 3 males and 3 females), and SE-7d (n=6; 3 males and 3 females); and in the *mTOR*$^{Cx3cr1\text{-}cre}$CKO groups: Sham (n=4; 2 males and 2 females), SE-1d (n=5; 2 males and 3 females), SE-3d (n=6; 3 males and 3 females), and SE-7d (n=4; 2 males and 2 females).

E. The time course of fold changes of TUNEL-positive cells (solid lines) and microglial density (dash lines) in control (gray) and *mTOR*$^{Cx3cr1\text{-}cre}$CKO mice (red).

F. Cell counts along the hippocampal pyramid layers of control and *mTOR*$^{Cx3cr1\text{-}cre}$CKO mice either sham-treated or 20 days post-SE. Sample sizes in the controls are: Sham (n=6; 3 males

JNeurosci Accepted Manuscript

and 3 females) and SE-20d (n=6; 3 males and 3 females); and in *mTOR*$^{Cx3cr1\text{-}cre}$CKO mice: Sham (n=6; 3 males and 3 females) and SE-20d (n=6; 3 males and 3 females).
Data are presented as mean + SEM. A two-tailed unpaired *t* test was used for the comparison between control and *mTOR*^{Cx3cr1}CKO mice.

Fig. 9 Impact of microglial mTOR deletion on the development of spontaneous recurrent seizures.
A. Schematic depiction of timelines of the video/EEG recording procedures.
B. Representative electrographic traces of spontaneous recurrent seizures (SRS) in sham- and pilocarpine-treated control and *mTOR*$^{Cx3cr1\text{-}cre}$CKO mice.
C. Percentage of mice that developed SRS in pilocarpine-treated control (n=33; 13 males and 20 females) and *mTOR*$^{Cx3cr1\text{-}cre}$CKO mice (n=24; 15 males and 9 females). None of the sham-treated control (n=13; 7 males and 6 females) and *mTOR*$^{Cx3cr1\text{-}cre}$CKO (n=8; 4 males and 4 females) mice developed SRS. $p< 0.0001$ for comparison in four groups and $p=0.0459$ between pilocarpine-treated control and *mTOR*$^{Cx3cr1\text{-}cre}$CKO mice by Chi-square test.
D & E: Seizure duration (D) and cumulative seizure events (E) in sham-treated control and *mTOR*$^{Cx3cr1\text{-}cre}$CKO mice and pilocarpine-treated control and *mTOR*$^{Cx3cr1\text{-}cre}$CKO mice. Data are presented as mean + SEM. $p < 0.0001$ by Mann-Whitney test between pilocarpine-treated control and *mTOR*^{Cx3cr1}CKO mice.

JNeurosci Accepted Manuscript

1149 **Table 1: Key resources, Related to Experimental Procedures.**

REAGENT or RESOURCE	SOURCE	IDENTIFIER
Antibodies		
Anti-Iba1	Wako	Cat#019-19741; RRID: AB_839504
Anti-Iba1	Novus Biologicals	Cat#NB100-1028; RRID: AB_521594
Anti-Ki67	Abcam	Cat#ab15580; RRID: AB_443209
Phospho-S6 Ribosomal Protein (Ser240/244)	Cell Signaling	Cat# 5364; RRID: AB_10694233
NeuN (D4G4O) XP® Rabbit mAb	Cell Signaling	Cat#24307; RRID: AB_2651140
Rat anti Mouse CD68	Bio-Rad	Cat#MCA1957; RRID: AB_322219
Anti-NeuN	Millipore	Cat#MAB377; RRID: AB_2298772
Anti-Glial Fibrillary Acidic Protein	Millipore	Cat#AB5541; RRID: AB_177521
Anti-VGluT2	Millipore	Cat#AB2251-I; *RRID*: AB_2665454
Anti-Homer1	Millipore	Cat#ABN37; *RRID*: AB_11214387
Anti VGAT	Synaptic Systems	Cat#131011; *RRID*: AB_887872
Anti Gephyrin	Synaptic Systems	Cat#147008; *RRID*: AB_2619834
Cleaved Caspase-3 (Asp175) (5A1E) Rabbit mAb	Cell Signaling	Cat#9664; RRID: AB_2070042
Goat anti-Rabbit IgG (H+L) Secondary Antibody, Alexa Fluor 488 conjugate	ThermoFisher	Cat#A-11034; RRID: AB_2576217
Goat anti-Rabbit IgG (H+L) Highly Cross-Adsorbed Secondary Antibody, Alexa Fluor 568	ThermoFisher	Cat#A-11036; RRID: AB_10563566
Goat anti-Rat IgG (H+L) Cross-Adsorbed Secondary Antibody, Alexa Fluor 555	ThermoFisher	Cat#A-21434; RRID: AB_2535855
Goat anti-Mouse IgG (H+L) Highly Cross-Adsorbed Secondary Antibody, Alexa Fluor 488	ThermoFisher	Cat#A-11029; RRID: AB_2534088
Goat anti-Chicken IgY (H+L) Secondary Antibody, Alexa Fluor 488	ThermoFisher	Cat#A-11039; RRID: AB_2534096
Donkey anti-Goat IgG (H+L) Highly Cross-Adsorbed Secondary Antibody, Alexa Fluor Plus 488	ThermoFisher	Cat#A32814; RRID: AB_2762838
Donkey anti-Goat IgG (H+L) Cross-Adsorbed Secondary Antibody, Alexa Fluor 647	ThermoFisher	Cat#A-21447; RRID: AB_2535864
Anti-mouse IgG, HRP-linked Antibody	Cell Signaling	Cat#7076; RRID: AB_330924
Anti-rabbit IgG, HRP-linked Antibody	Cell Signaling	Cat#7074; RRID: AB_2099233
Anti-PE MicroBeads	Miltenyi	Cat#130-105-639
anti-Cx3cr1-PE antibody	Biolegend	Cat#149006; *RRID*: AB_2564315
Chemicals, Peptides, and Recombinant Proteins		
Rapamycin	LC Laboratories	Cat#R-5000
Bovine Serum Albumin	Millipore Sigma	Cat#A7030
Donkey serum	Millipore Sigma	Cat#D9663; RRID: AB_2810235
pHrodo™ Green Zymosan Bioparticles™ Conjugate for Phagocytosis	ThermoFisher	Cat#P35365
Fluoro-Jade B ®	Histo-Chem Inc	Cat#1FJB
Cresyl Violet acetate	Millipore Sigma	Cat#C5042
Pilocarpine hydrochloride	Millipore Sigma	Cat#P6503
(−)-Scopolamine methyl bromide	Millipore Sigma	Cat#S8502
Diazepam	Millipore Sigma	Cat#439-14-5
DAPI	Millipore Sigma	Cat#D9542
Percoll	GE Healthcare	CAT#17-0891-01
Papain	Sigma	CAT#P3125
Dispase II	STEMCELL	CAT#07913
TRIzol	Life technologies	CAT#15596018
glycogen	Roche,	Cat#10901393001
DPX	Sigma	CAT#06522
RNase-free water	Fisher Scientific,	Cat#BP561-1

JNeurosci Accepted Manuscript

Critical Commercial Assays		
In Situ Cell Death Detection Kit, TMR red	Millipore Sigma	Cat#12156792910
Verso cDNA Synthesis Kit	ThermoFisher	AB1453B
PowerUp™ SYBR™ Green Master Mix	ThermoFisher	A25777
Other Materials		
Three-channel EEG electrodes	Plastic ONe	Cat#MS333/3-AIU/SPC
MS Columns	Miltenyi	Cat#130-042-201
Pre-Separation Filters (30 µm)	Miltenyi	Cat#130-041-407
Falcon® 40µm Cell Strainer	Corning	CAT#352340
PCR plate	Bio-Rad,	CAT#MLL9601
Gelatin-subbed slides	SouthernBiotech	CAT#SLD01-CS
Experimental Models: Organisms/Strains		
Tg(Cx3cr1-cre)MW126Gsat/Mmucd (Cx3cr1-cre) mice	MMRRC	Strain# 036395-UCD; RRID: MMRRC_036395-UCD
B6.129S4-Mtor$^{tm1.2Koz}$/J (mTOR$^{f/f}$) mice	The Jackson Laboratory	Strain# 011009; RRID: IMSR_JAX:011009
C57BL/6NJ (*WT*) mice	The Jackson Laboratory	Strain#005304; RRID: IMSR_JAX:005304
Software and Algorithms		
ImageJ	NIH	https://fiji.sc/ or https://imagej.nih.gov/ij/
GraphPad Prism 7.0	GraphPad Software	https://www.graphpad.com
Zen Black	Zeiss	https://www.zeiss.com
Zen Blue	Zeiss	https://www.zeiss.com
Neurolucida	MBF bioscience	http://www.mbfbioscience.com
Bitplane	IMARIS software	https://imaris.oxinst.com/
DataWave SciWorks	DataWave	http://www.dwavetech.com

Table 2. Primers used in this paper, Related to Experimental Procedures.

Primers used for quantitative Real-Time PCR:			
Gene	Sense (5′–3′)	anti-sense (5′–3′)	Species
TNFa	ATGGCCTCCCTCTCATCAGT	GTTTGCTACGACGTGGGCTA	Mouse
IL-1b	CGCAGCAGCACATCAACAAG	GTGCTCATGTCCTCATCCTG	Mouse
IL-6	ACCAGAGGAAATTTTCAATAGGC	TGATGCACTTGCAGAAAACA	Mouse
IFNb	TCCGAGCAGAGATCTTCAGGAA	TGCAACCACCACTCATTCTGAG	Mouse
GAPDH	GACAACTTTGGCATTGTGG	ATGCAGGGATGATGTTCTG	Mouse
Genotype primers:			
Mouse strains	Forward (5′–3′)	Reverse (5′–3′)	
Cx3CrCre+/-	GATCCTGGCAAATTTCGGCTA	TTGCCTGCATGACCGGTCGA	Mouse
mTOR flox	GATAATTGCAGTTTTGGCTAGCAG	CTCCTTCTGTGACATACATTTCCT	Mouse

JNeurosci Accepted Manuscript

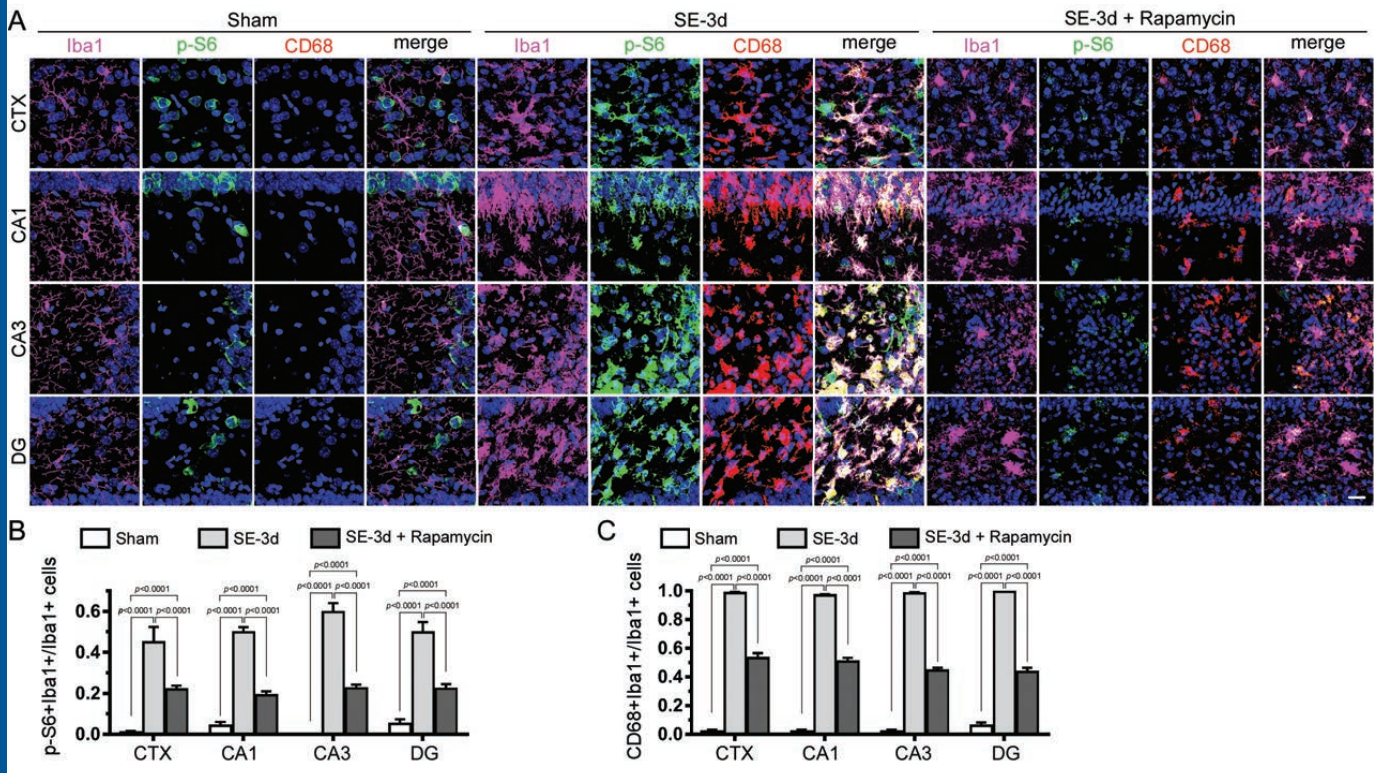

JNeurosci Accepted Manuscript

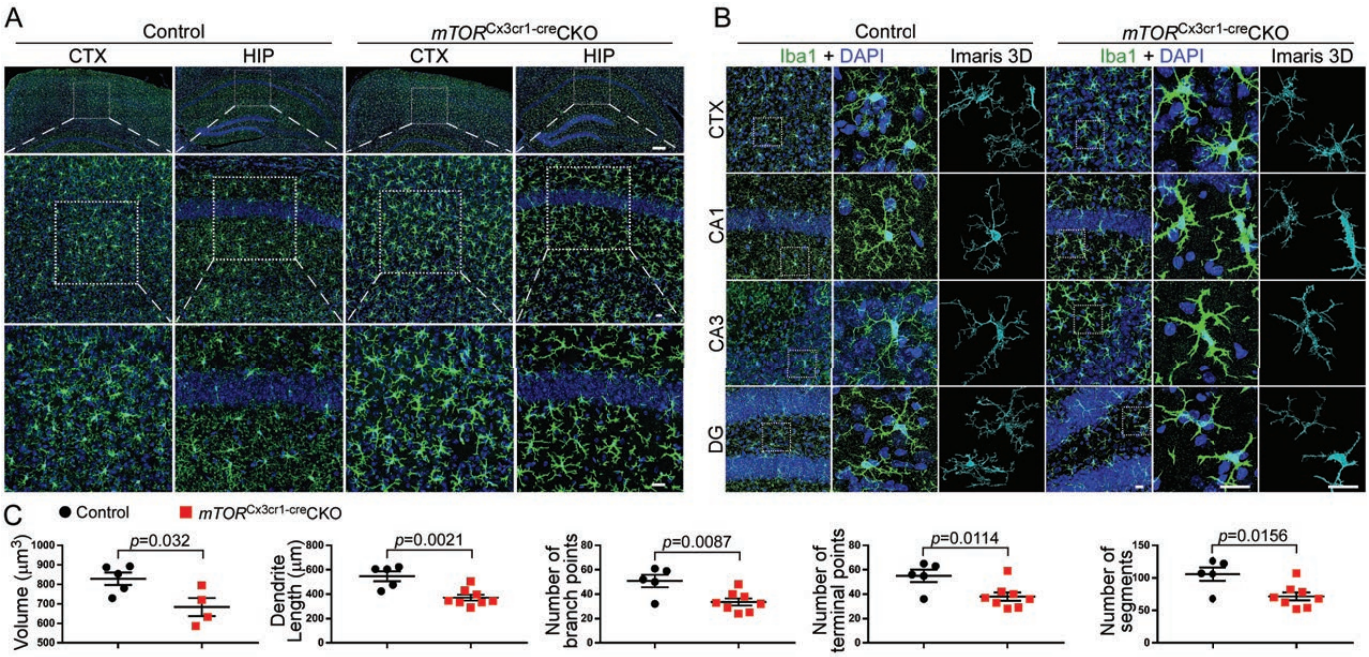

JNeurosci Accepted Manuscript

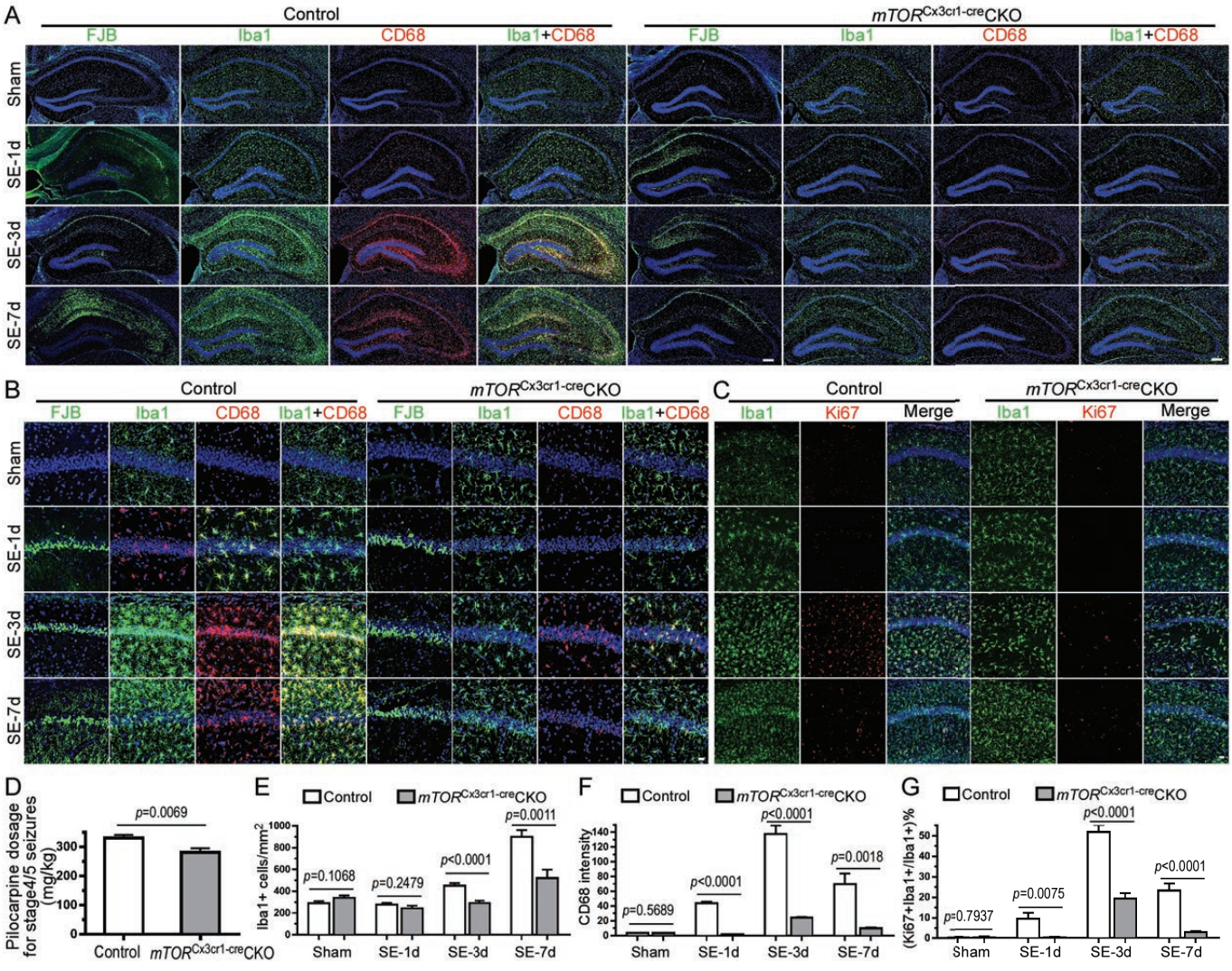

JNeurosci Accepted Manuscript

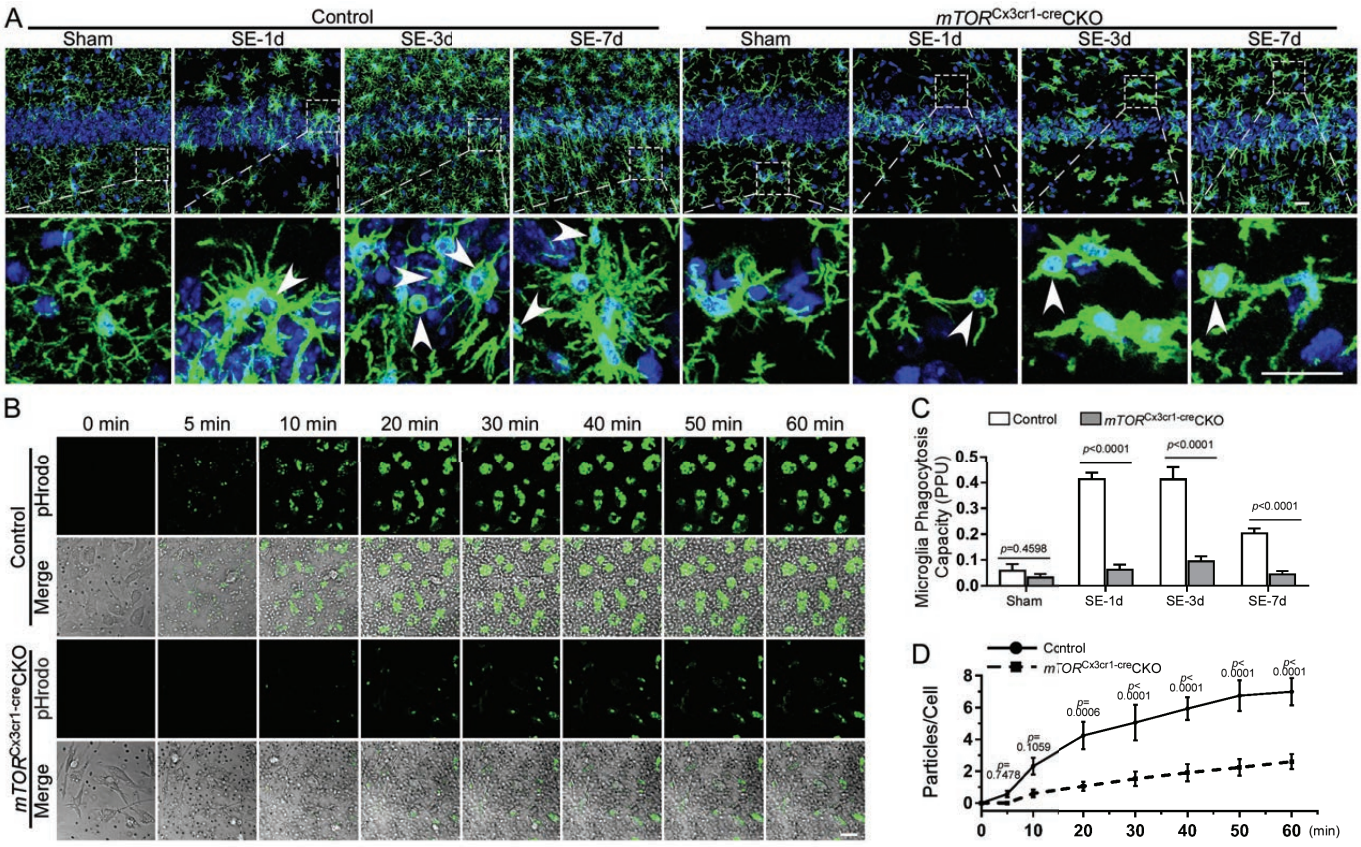

JNeurosci Accepted Manuscript

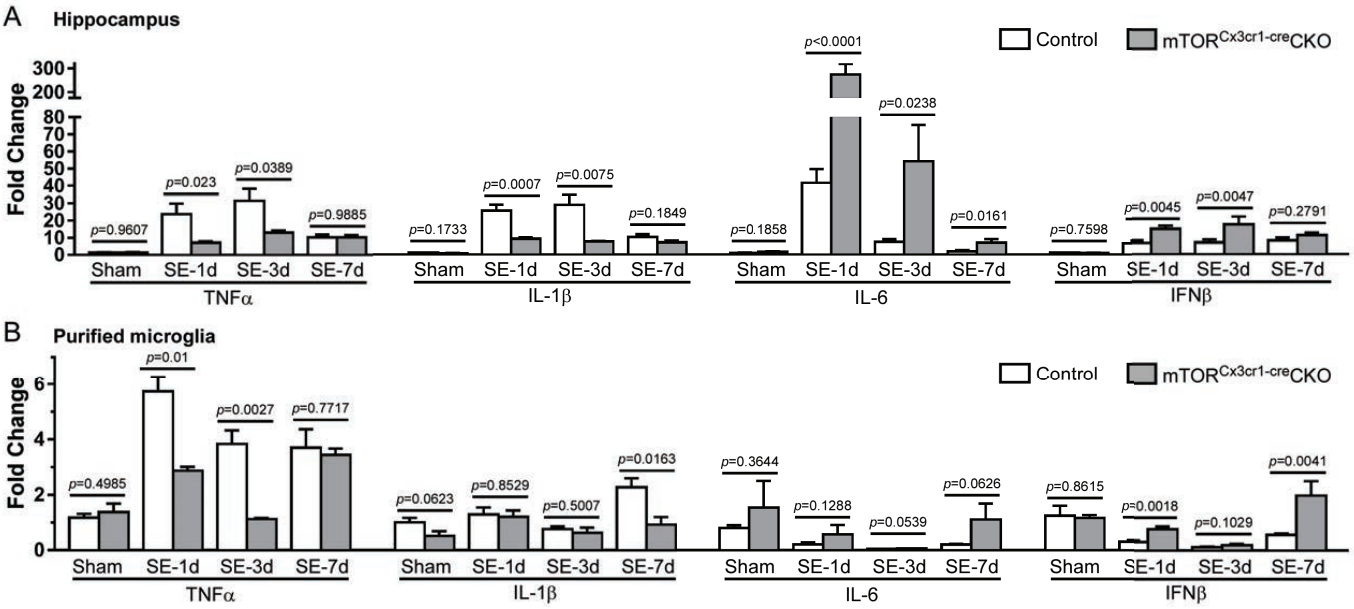

JNeurosci Accepted Manuscript

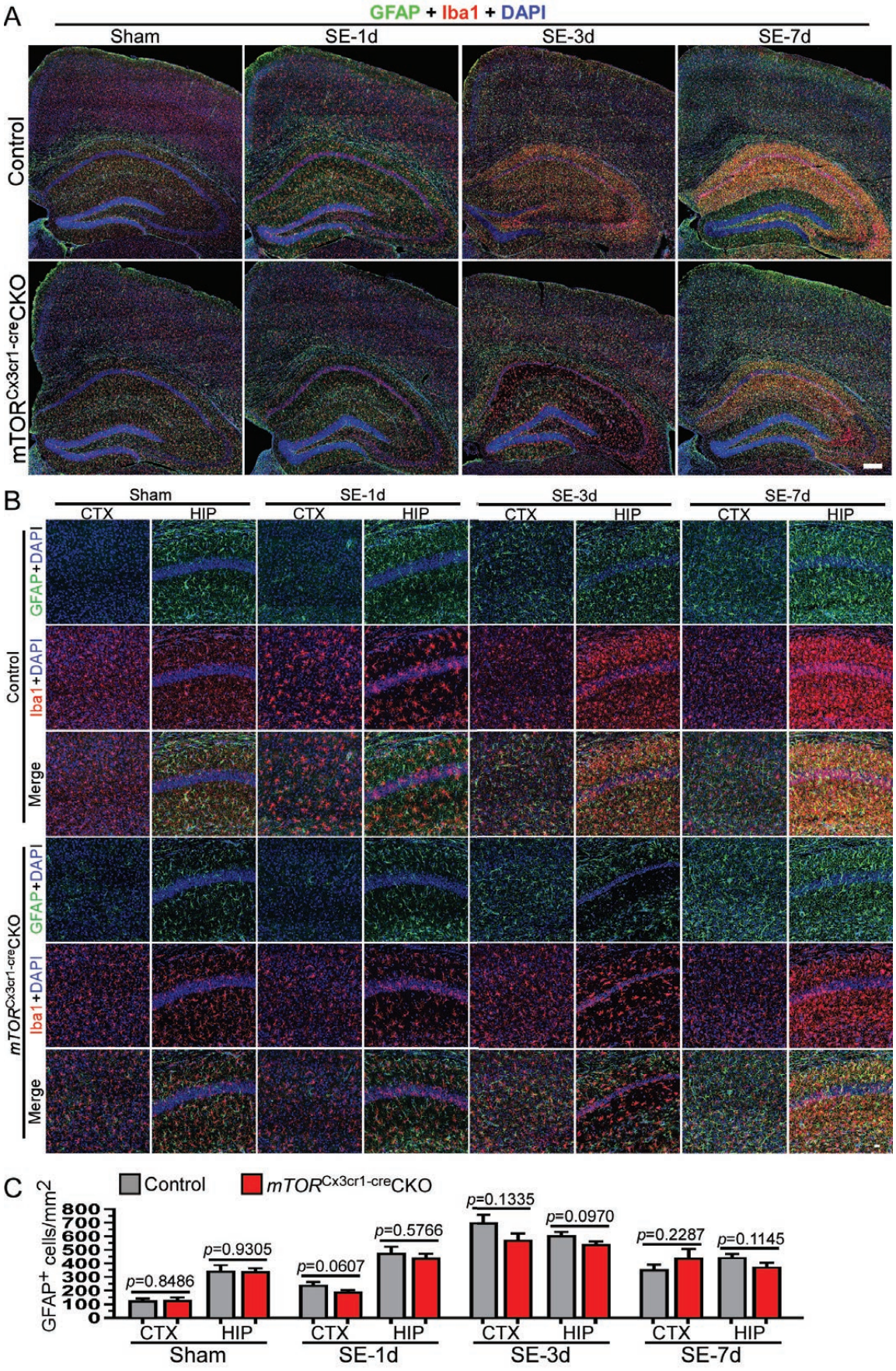

JNeurosci Accepted Manuscript

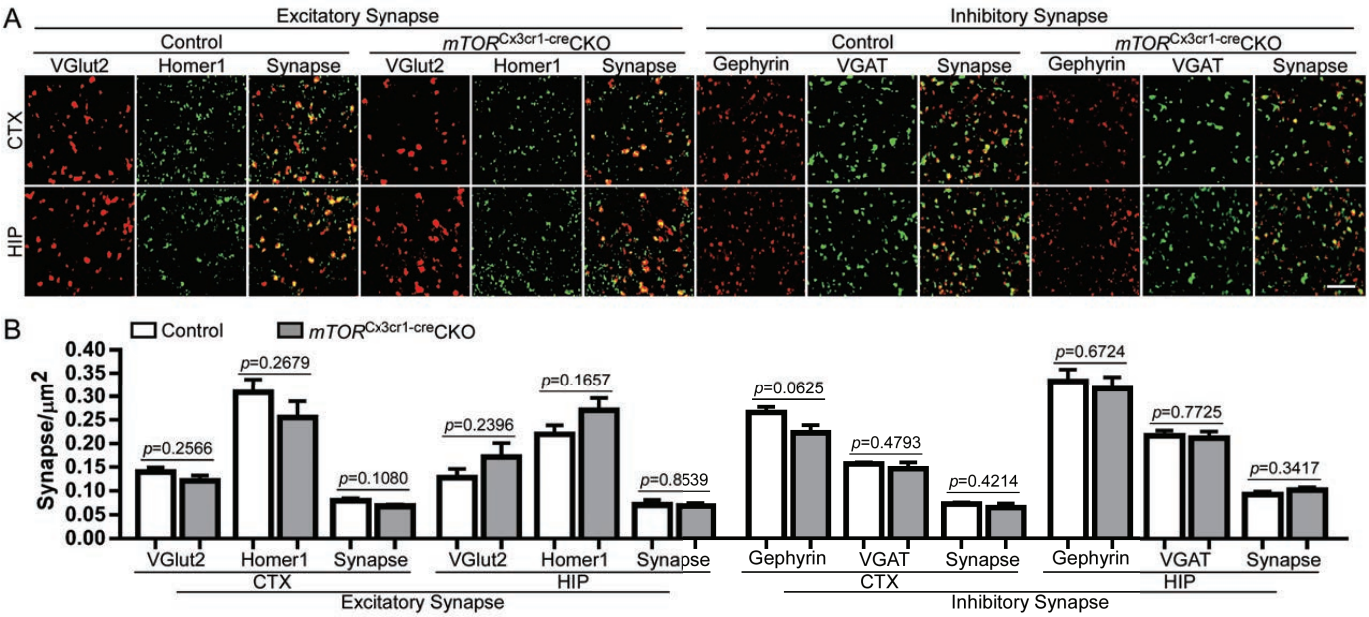

JNeurosci Accepted Manuscript

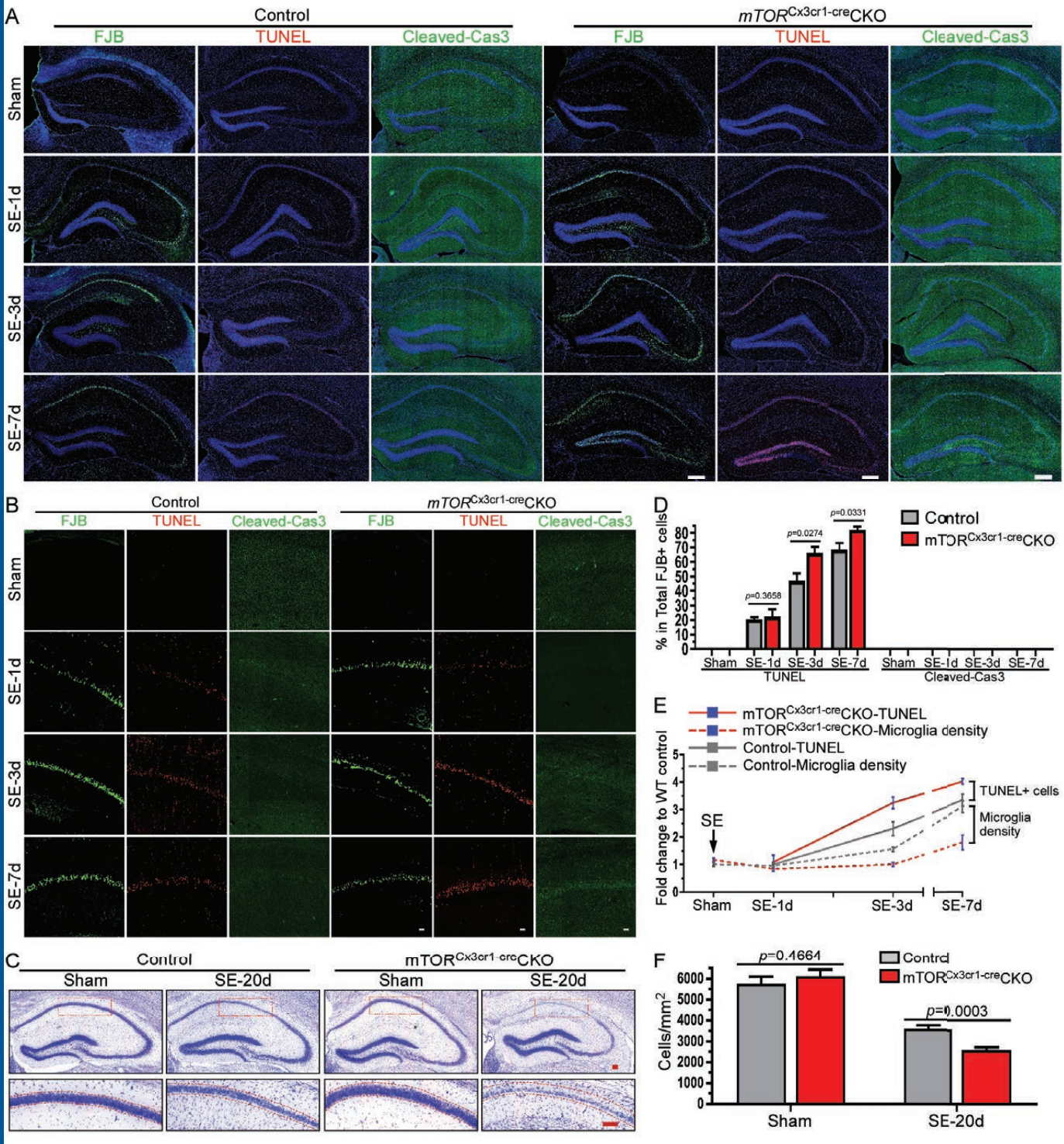

JNeurosci Accepted Manuscript